ABSTRACT

Title of Thesis:	PERFORMANCE INVESTIGATION OF CHP EQUIPMENT
	Ji Bian, Master of Science, 2005
Thesis Directed By	Professor Reinhard Radermacher, Ph.D. Department of Mechanical Engineering

The Cooling Heating & Power systems for Buildings (BCHP) are attracting more attention due to their advantages as compared to conventional energy systems. As a developing technology, there are still problems to be solved. Fuel flexibility and dynamic response between different machines in the system are two of the main issues to be investigated.

This study presents research conducted on a BCHP system that is composed of a microturbine, an absorption chiller and a solid desiccant unit that are driven by the microturbine's exhaust gas to provide cooling and dehumidification. It demonstrates the feasibility of operating the microturbine that is originally designed for natural gas on propane and analyzes the reasons for the efficiency reduction when operating on propane. It further presents a model that describes the transient behavior of the absorption chiller, which requires a much longer period to reach its steady state compared with the microturbine.

PERFORMANCE INVESTIGATION OF CHP EQUIPMENT

By

Ji Bian

Thesis submitted to the Faculty of the Graduate School of the
University of Maryland, College Park, in partial fulfillment
of the requirements for the degree of
Master of Science
2005

Advisory Committee:
Professor Reinhard Radermacher, Chair/Advisor
Assistant Professor Elias Balaras
Assistant Professor Bao Yang

Dedication

To my parents, for loving me just the way I am.

Acknowledgement

My thanks and sincere appreciation goes to Dr. Reinhard Radermacher for providing me the opportunity to continue my education. His wisdom and patience have guided me in my research and helped me with every little step that I made. This work wouldn't be possible without his understanding and encouragement. I sincerely appreciate all the advice that I got from him, and believe that in the future, that advice will be as precious as it is now, if not more so.

I am also grateful for all the help that Xiaohong Liao gave me, it was a great pleasure working with her and I did learn a lot. Special thanks go to CHP team members, Dennis Moran, Sandeep Nayak, and Shenglan Xuan.

Finally, I would like to express my gratitude to everyone in CEEE, my family and friends, for their support and encouragement.

TABLE OF CONTENTS

1 Introduction 1

Combined Heat and Power 1

Cooling Heating & Power Systems for Building 2

2 UMD CHP Test Center 4

Chesapeake Building 4

MT-Based CHP system 5

Overview 5

Equipment 7

System Integration 11

System Control and Data Acquisition 14

3 Motivation and Objectives 20

Motivation 20

Objectives 21

4 Microturbine Fuel Flexibility 23

Overview and introduction 23

Microturbine 23

The Microturbine in the MT-Based CHP System 25

Properties of Fuels 32

Natural Gas 32

Propane 33

Comparison 35
Experimental Setup 35
Natural Gas Test 36
Propane Test 36
Control software settings 40
Data collection 42
Data Processing 43
Fuel flow rate 44
Unit Volume Conversion 44
Initial Calculation 45
Further Analysis of Efficiency Degradation 49
Fuel Control Analysis 50
Gas Mass Flow Rate of the 60 kW MT 52
30 kW MT Calculation 54
Exhaust Heat Analysis 57
Observation 57
Exhaust Heat for Building Cooling 59
Suggestions 62
5 Absorption Chiller Transient Model 64
Introduction to absorption technology and absorption chiller 64
Absorption Chiller in the MT-Based CHP System 67

Model Description 70

Assumptions 70

Modeling of Components 71

Integration of Components Models 79

Modeling Tool 80

Simulink Blocks 80

Results and Discussions 81

6 Conclusions 89

MT Fuel Flexibility 89

Absorption Chiller Transient Simulation 90

7 References 91

LIST OF FIGURES

Figure 1 The Chesapeake Building on the University of Maryland-College Park Campus 4

Figure 2 The MT-Based CHP System 6

Figure 3 P & I Diagram for MT-Based CHP System 6

Figure 4 The 60kW Microturbine 7

Figure 5 Schematic Layout of the Solid Desiccant Unit 9

Figure 6 SDU Performance Profile on a Typical Summer Day 11

Figure 7 Exhaust Temperature Profile on a Typical Summer Day 12

Figure 8 Comparison of Grid Electric System and Chesapeake System[17] 13

Figure 9 JACE Control Web-based Interface of MT-Based BCHP System and RTU #2 15

Figure 10 DAS User Interface 16

Figure 11 A Sample Calibration of Humidity Sensors 19

Figure 12 Schematic of Microturbine 23

Figure13 T-S Diagram 25

Figure 14 Schematic of the 60 kW Microtubine 26

Figure 15 Microturbine Generator 27

Figure 16 60 kW Microturbine Operating Statepoints 27

Figure 17 60 kW Microturbine Performance Comparison at Full Load 28

Figure 18 MT Power Output vs. Compressor Inlet Temperature 29

Figure 19 MT Efficiency vs. Compressor Inlet Temperature 29

Figure 20 Engine Speed vs. Compressor Inlet T. 30

Figure 21 Compressor Inlet Temperature vs. Ambient Temperature 31

Figure 22 P-h Diagram of Methane 33

Figure 23 P-h Diagram of Propane 35

Figure 24 Coalescing Filter 37

Figure 25 Natural Gas Regulator and Propane Regulator (Test year one) 38

Figure 26 Regulators on the Pipeline (Test year two) 39

Figure 27 Pressure Settings 39

Figure 28 Propane Pipeline with Heat Trace and Insulation 40

Figure 29 Fuel Setting Panel 41

Figure 30 MT Performance on Typical Days 43

Figure 31 Power Output vs. Compressor Inlet Temperature 45

Figure 32 MT Net Power Efficiency Comparison 46

Figure 33 MT Parasitic Power Consumption Comparison 47

Figure 34 Efficiency of Gross Power Comparison 49

Figure 35 Mass Flow Rate Comparison 53

Figure 36 Ratios Comparison 54

Figure 37 Ratio Comparison w/ 30 kW MTAssumption 56

Figure 38 Comparison of the Amounts of Waste Heat 58

Figure 39 Idealized Load Profiles for Cooling Heating and Power[11] 60

Figure 40 Real Building Load Profile (heating season)[11] 61

Figure 41 Real Building Load (cooling season)[11] 61

Figure 42 Diagram of Single Effect Absorption Chiller 65

Figure 43 Schematic of the Single Effect Chiller 68

Figure 44 Exhaust Heat Management and Safety Control of the MT-Based CHP System 69

Figure 45 Schematic of Solution Heat Exchanger 72

Figure 46 Schematic of Desorber/Condenser Pair 74

Figure 47 Schematic of Evaporator & Absorber 77

Figure 48 Chilled Water Temperature Profile 83

Figure 49 Cooling Capacity Profile 84

Figure 50 Chiller Temperature Profiles 85

Figure 51 Chiller Pressure Profile 86

Figure 52 Concentration of Strong Solution 87

Figure 53 Exhaust Gas Outlet Temperature 88

LIST OF ABBREVIATIONS

BCHP	Combined Cooling, Heating and Power for Buildings
CHP	Combined Cooling, Heating and Power
DAS	Data Acquisition System
EES	Engineering Equation Solver
HHV	Higher Heating Value
HP VEE	Hewlett-Packard Visual Engineering Environment
LHV	Lower Heating Value
LiBr	Lithium Bromide
MT	Microturbine
NG	Natural Gas
RTU	Roof Top Unit
SDU	Solid Desiccant Unit
UA	Over All Heat Transfer Coefficient
VAV	Variable Air Volume

1 Introduction

Combined Heat and Power

Combined Heat and Power (CHP) technologies produce both electricity and heat from a single fuel at a facility located near the consumer. A typical CHP system is usually composed of an electric generation device which also provides a certain amount of waste heat at the same time. The waste heat will then be utilized to drive a series of thermally activated devices, e.g., absorption chiller integrated with a desiccant wheel.

Comparing a CHP system with conventional electricity generators, it has several advantages.

Firstly: Energy efficiency enhancement. In conventional power generation devices, a single fuel can be used only to provide either power or heat. That is, to provide power and heat, more fuel has to be consumed with traditional electricity generation than with CHP system. On the other hand, since most equipment produces electricity with a heat engine, there is always waste heat rejected. With the application of CHP technologies, the heat that would otherwise be rejected as waste heat can be utilized to provide heating, cooling, steam, hot water, dehumidification, or other benefits. For example, a state-of-the-art central plant (a combined cycle plant using natural gas) offers maximum system fuel efficiency for delivered power in the range of 55-60%. Under common circumstances, CHP systems will achieve efficiencies exceeding 70%. CHP systems achieving efficiencies exceeding 80% are frequent, and some systems have been shown to reach levels in excess of 90%[2]. In

addition, by providing on-site power, CHP systems also eliminate the need for large power grids, which reduces transmission and distribution line losses as well.

Another benefit of CHP systems is that they are environmentally benign. Most CHP Systems use natural gas as their fuel. Compared to coal, which is widely used by traditional power generation, natural gas is a much cleaner source. Generally, natural gas produces about 40% less NO_x and 67% less CO_2 than coal, though it is more expensive.

Cooling Heating & Power Systems for Building

The use of CHP systems falls into three major categories: industrial, district energy and commercial buildings. Cooling Heating and Power system for Building (BCHP) comes into play in the last category. Usually, these systems have a "smaller size", that is, their generation capacity is normally less than 1 MW. With these systems, the buildings can have their own on-site power generation, accompanied by cooling and heating, utilizing the waste heat generated in the process of power generation.

A BCHP system is usually composed of a power generation device (prime mover), followed by a series of heat-activated units. For small scale power generation required in BCHP, some promising and emerging technologies such as microturbines and fuel cells can be used in addition to conventional reciprocating engine generators. Absorption chillers and desiccant units are commonly used as heat-activated equipment that utilize the waste heat produced by the power generation equipment.

Similar to their larger counterparts, BCHP can also contribute to energy savings and have environmental benefits. Previous research shows that the savings from CHP technology in commercial buildings will account for nearly two-thirds of a quadrillion Btu (Quads) of energy and 23 million tons of carbon emissions[4].

2 UMD CHP Test Center

Chesapeake Building

The UMD BCHP test center is located in the Chesapeake Building on the University of Maryland-College Park campus. Built in 1991 and used as an administrative office building, the Chesapeake Building has four floors with a total floor space of 4700 square meters, and can represent 23% of US office space. The building is divided into two air conditioning zones, each of which comprises two floors.

Figure 1 The Chesapeake Building on the University of Maryland-College Park Campus

When the building was first built, the air-conditioning of the building was entirely supplied by two roof top units (RTU), one for each zone. The heating/reheating is controlled by the electric heaters inside the variable air volume (VAV) units and with

electric base board heat around the perimeter zone.

After the installation of the two CHP systems, each RTU works with one CHP system. The respective RTU provides additional cooling capacity whenever the capacity of the CHP system is insufficient. The cooling load is thus shared by these two new CHP systems.

MT-Based CHP system

Overview

One of the two CHP systems mentioned in the last section is a microturbine based system. It is composed of a microturbine, an absorption chiller and a solid desiccant unit as shown in Figure 2.

The microturbine is the prime mover of this system; it generates electricity and produces exhaust gas. The exhaust gas is used to drive the absorption chiller, and the remaining heat in the exhaust gas is then used by the solid desiccant unit for regeneration.

This system cooperates with RTU #2 to condition 3000cfm supply air for the lower two floors of the building. The microturbine also provides all parasitic power required by the absorption chiller and the desiccant system.

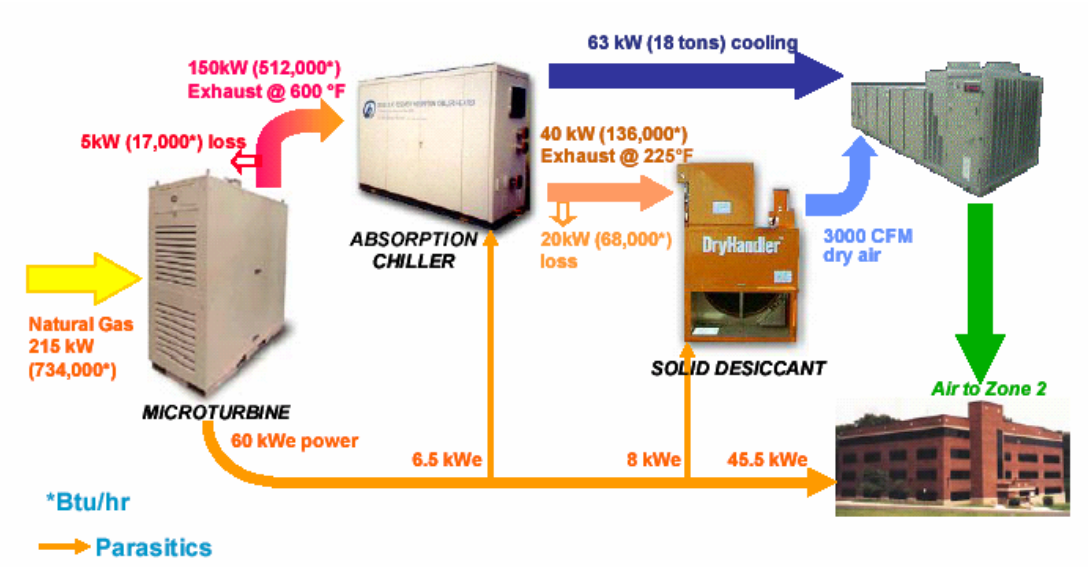

Figure 2 The MT-Based CHP System

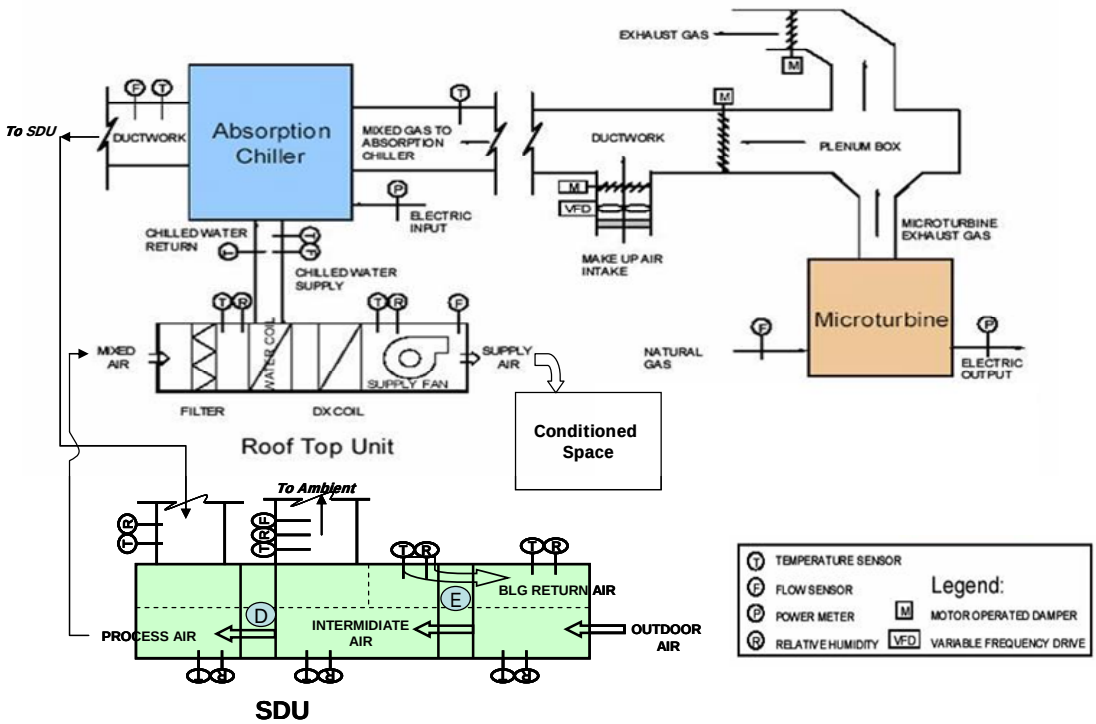

Figure 3 P & I Diagram for MT-Based CHP System

Figure 3 shows the process and instrumentation of the MT-Based CHP System. As

can be seen in this schematic, the connection between the MT and the chiller includes a duct, damper, actuator, and fans.

After coming out of the microturbine, part of the exhaust gas is mixed with ambient air and flows into the absorption chiller, while the other part is dumped into the ambient. The cooling coil through which the chilled water of the absorption chiller runs is placed in serial with the original DX coil of the RTU #2. The process air flows through the chiller's cooling coil and DX coil consecutively, be cooled, and then supplied into the building.

Equipment

1, Microturbine

Figure 4 The 60kW Microturbine

Serving as the prime mover in the whole system, the microturbine works on a Brayton

Cycle, converts natural gas into electric power, while consuming a relatively small amount of parasitic power (~ 4kW).

Rated Electrical Output	60 kW
Rated Electrical Efficiency	27% (LHV)
Parasitic Electric Consumption	~1 kW
Approximate Actual Output	59 kW
Approximate Electrical Efficiency at ISO	26.5% (LHV)
Exhaust Temperature	320°C

Table 1 Technical Data for the 60kW Microturbine

2, Absorption Chiller

A direct fire, single effect, LiBr absorption chiller is used in the system. It connects with the MT by a duct through which the exhaust gas is delivered to drive the chiller. The chilled water provided by the absorption chiller flows through a cooling coil that is inserted in the air stream directly before the original direct expansion (DX) coil of RTU#2.

Cooling capacity	kW (RT)	75 (21)
Heating capacity	kW (MBH)	90 (307)
Chilled water outlet/inlet temp.	°C (°F)	7.2 (45) / 12.2 (54)
Heating water outlet/inlet temp.	°C (°F)	50 (122) / 43.9 (111)
Chilled water flow rate	m^3/h (GPM)	12.7 (56)
Exhaust inlet temp.	°C (°F)	230 / 590
Exhaust flow rate	kg/s (lb/h)	0.49 (3885)
Parasitic power	kW	5.78
Weight	kg (lb)	1900 (4185)

Table 2 Technical Data of the 21-ton Absorption Chiller

3, Solid Desiccant Unit

The exhaust gas, which has a temperature about 105 °C after driving the absorption chiller, will then be utilized by a solid desiccant unit. Ideally, these two units should stand as close to each other as possible, to minimize the heat loss of the exhaust gas during transportation. However, due to the weight support limit of the roof top, only the desiccant unit can be put on the roof, while the chiller and MT have to stay on the ground. This made the duct from the chiller to the desiccant unit quite long (106m) that the amount of heat loss through the duct can reach up to 20 kW and thus cannot be neglected.

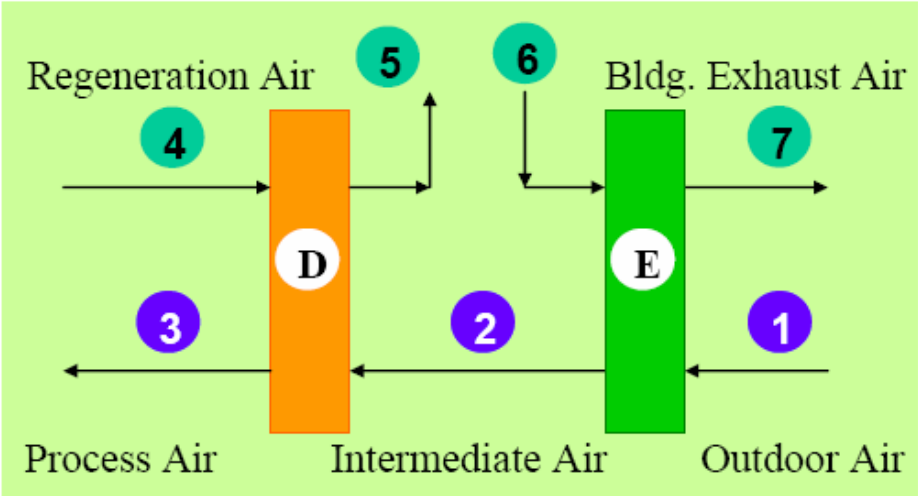

Figure 5 Schematic Layout of the Solid Desiccant Unit

As shown in Figure 5, there are a desiccant wheel Ⓓ and an enthalpy wheel Ⓔ in

the unit, and a total of three air streams flowing through: regeneration air, exhaust air, and process air.

The outdoor air comes into the SDU, and firstly exchanges enthalpy with building exhaust air, which comes from the ventilation of the building. After that, this air stream, which is called intermediate air, flows through the desiccant wheel, where it is dehumidified and then becomes process air for the building. The desiccant wheel is then dried by the regeneration air, which, in our case, is the exhaust gas after the chiller. In addition to using exhaust gas, the heat that is needed by the unit could also be provided by a built-in burner.

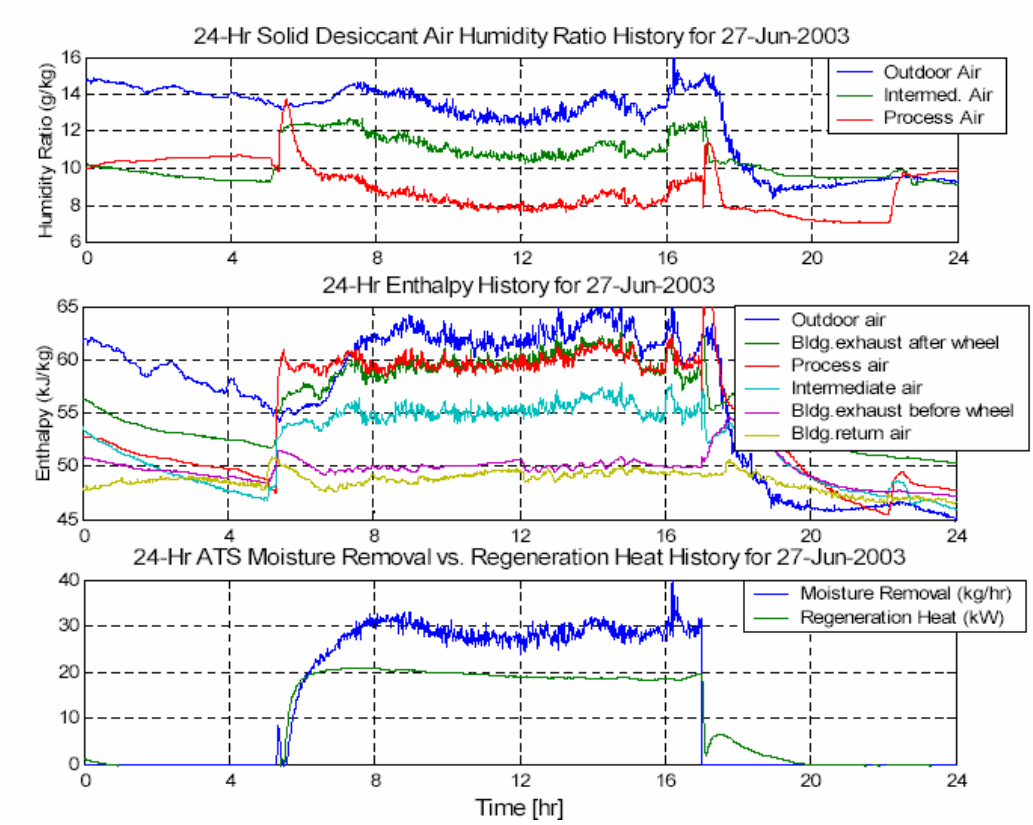

Figure 6 SDU Performance Profile on a Typical Summer Day

The plot in Figure 6 shown above is the performance profile of the solid desiccant unit on a typical summer day. The moisture of the outdoor air is removed by the enthalpy wheel through the enthalpy exchange with the building exhaust air and the desiccant wheel which is regenerated by the exhaust consecutively . Also the SDU has a moisture removal capability of around 30kg/hr at its steady state, providing 20 kW regeneration heat.

System Integration

In this system, the 60kW microturbine serves as the prime mover, providing both power and heat with a power generation efficiency of around 27%. The exhaust gas, which is about 300 °C, will be used to drive the absorption chiller, which provides cooling to the supply air together with RTU #2. When leaving the absorption chiller, the exhaust gas still has a temperature of about 105 °C, and will be delivered into the desiccant unit, which is used to dehumidify the air.

Figure 7 depicts the exhaust gas and its temperature levels flowing through each component on a typical summer day, with SI and English units shown on the left and right y axis. Point ① represents the exhaust entering the absorption chiller; points ② and ③ represent the exhaust leaving the absorption chiller and entering the desiccant wheel respectively; point ④ shows the exhaust leaving the desiccant wheel

and point ⑤ represents the ambient temperature. The temperature drop between point ② and ③ is caused by the long duct between the absorption chiller on the ground and the desiccant unit on the roof top that is mentioned above. It can be observed that from 140kW exhaust gas leaving the MT, 66% (~92kW) were consumed by the absorption chiller, 16% (~22kW) consumed by the solid desiccant unit, and the rest were lost to the ambient, during exhaust gas transportation and after the desiccant unit.

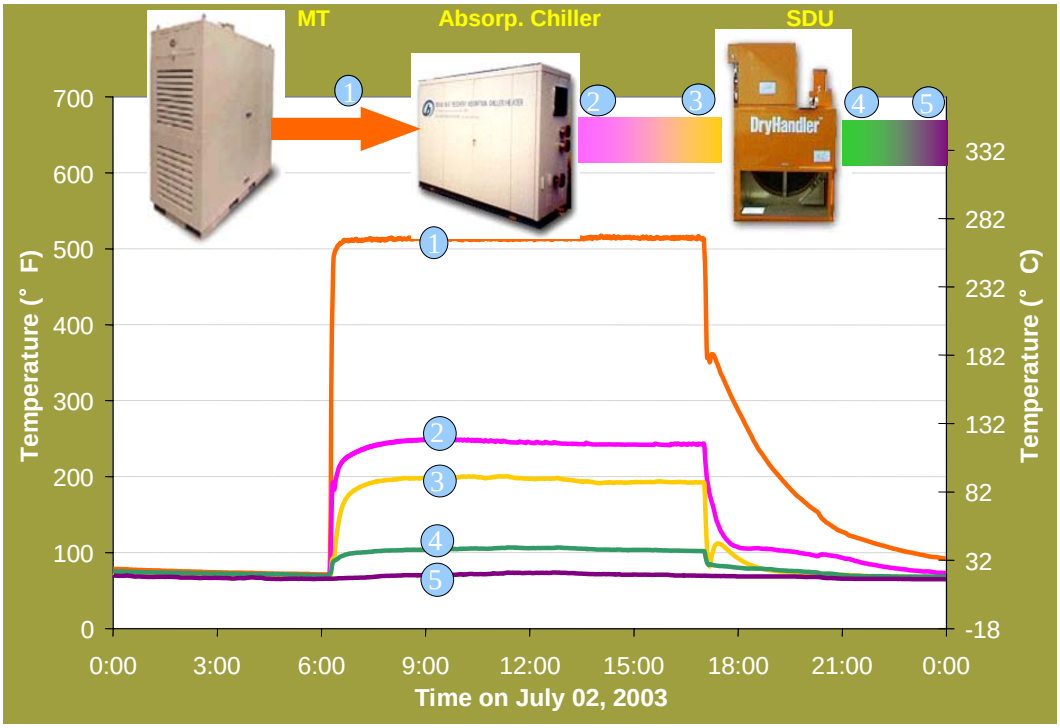

Figure 7 Exhaust Temperature Profile on a Typical Summer Day

Compared to drawing power directly from the grid for cooling, MT-Based BCHP shows an energy saving potential for the same amount of power generation and cooling capacity. Figure 8 shows a simple calculation for both the conventional

system and the BCHP system, of how much primary energy each of them would require to provide the same amount of electricity and cooling capacity.

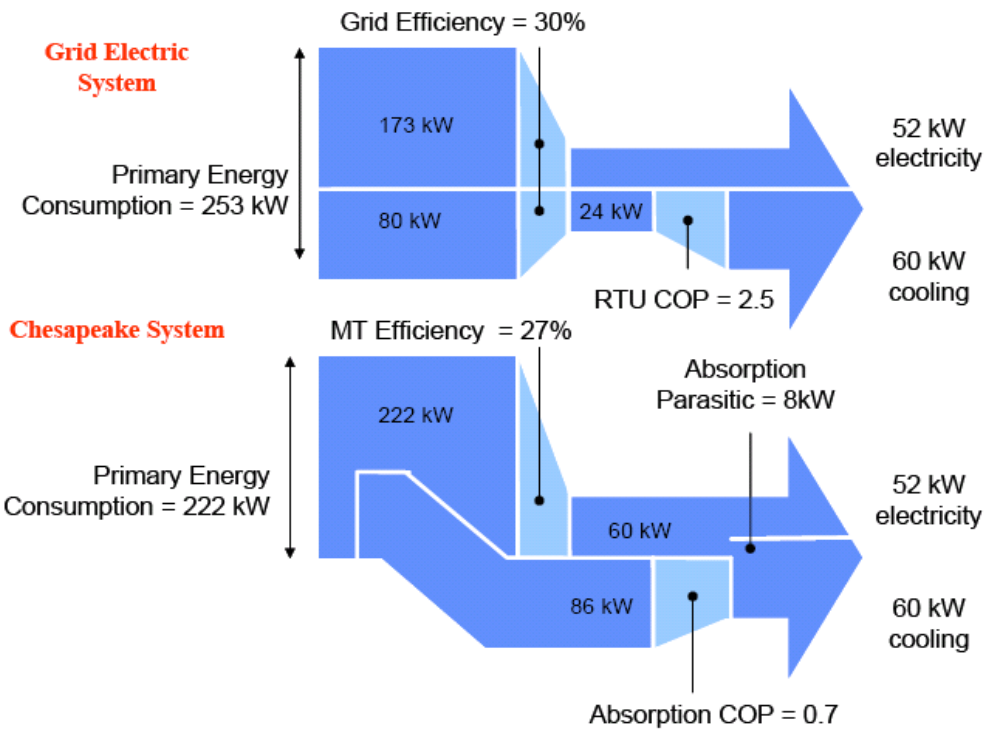

Figure 8 Comparison of Grid Electric System and Chesapeake System[17]

Both systems shown in Figure 8 are providing 52 kW electricity and 60 kW cooling to the building.

In the grid electric system, with a 30% grid power production and delivery efficiency, 173 kW primary energy consumption is needed to provide 52 kW electricity. To satisfy the 60 kW cooling, the Roof Top Unit (RTU) that has a coefficient of performance (COP) of 2.5 [Marantan, 2002] needs 24 kW of electricity, which, when

drawn directly from the grid, requires 80 kW of primary energy. Thus, the primary energy consumption adds up to 253 kW for the grid electric system.

With the Chesapeake System, the electricity is generated by the microturbine which has an efficiency of 27%. Besides the 52 kW of electricity that the building needs, the MT needs to generate another 8 kW of electricity to be used by the absorption chiller, which provides cooling to the building. The absorption chiller has a COP of 0.7 and thus requires a waste heat input of 86 kW to provide 60 kW of cooling, which the MT's exhaust heat can always provide. So, the primary energy that the Chesapeake CHP system requires is what the MT requires to output 60 kW of electricity, and that is 222 kW, which is 31 kW or 12% less than what is needed by the grid electric system. The primary energy requirement would be even lower, if the parasitic power could be reduced or eliminated. In the best possible case that the 8 kW parasitic power was eliminated, the primary energy savings would be 24%.

System Control and Data Acquisition

1. Control

A Tridium Niagara Framework Building Control System is implemented for controlling of the BCHP systems in the Chesapeake Building. Through a Java Application Control Engine (JACE), which can communicate with an array of logic controllers and directly interact with the RTUs and CHP Systems, the control and

status monitoring is accessible through the web.

As shown below in Figure 9, the two systems can both be monitored and controlled on one screen. The alarm function of the JACE controller allows the user to set up alarms for abnormal conditions, and it can automatically send out e-mails to notify the users so that most prompt reaction can be made to these conditions. Meanwhile, an operation schedule for the systems is also set up to minimize the energy loss.

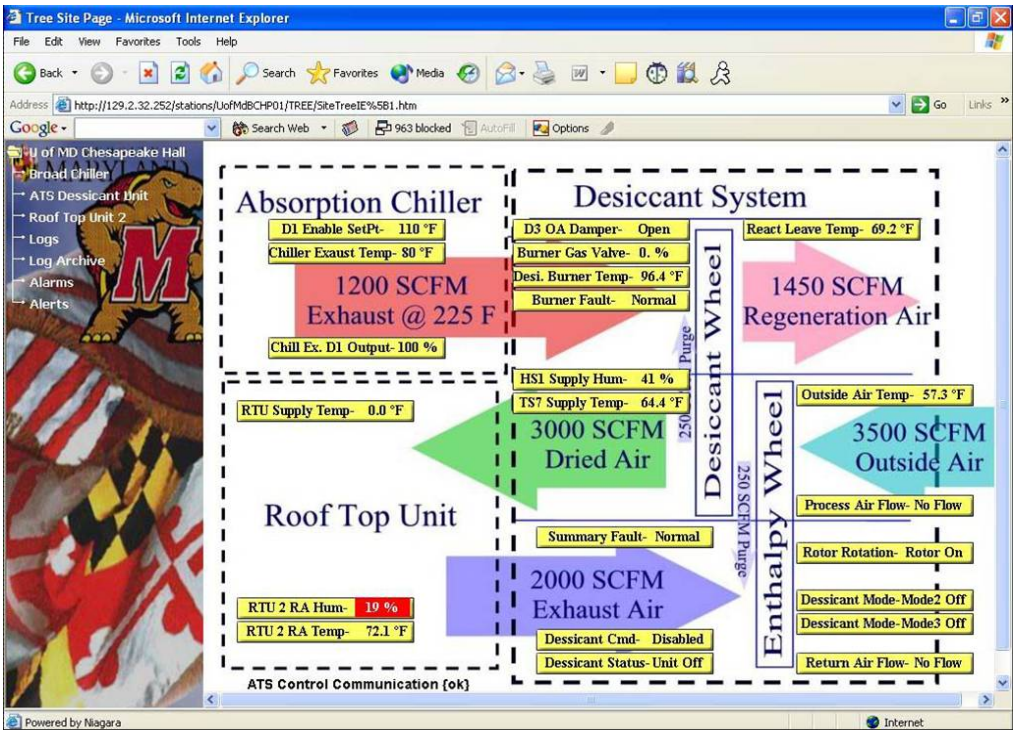

Figure 9 JACE Control Web-based Interface of MT-Based BCHP System and RTU #2

2. Data Acquisition System

A data acquisition system (DAS) is installed to measure all relevant temperatures, relative humidities, pressures, flow rates, and power consumptions to calculate the

performance of the building and the CHP systems under all operating conditions. This data acquisition system is completely separated from the control system. Because all of the measurement routines and programs are custom programmed by the user in the HP VEE (Hewlett-Packard Visual Engineering Environment), the readings that this DAS provides can be completely customized.

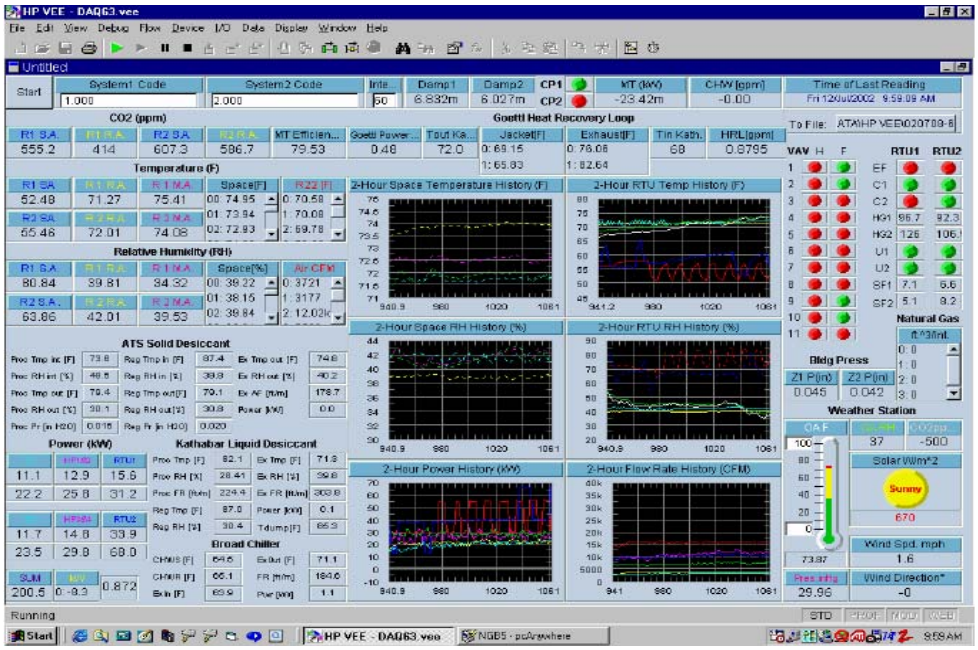

Figure 10 DAS User Interface

A total of 131 sensors are spread all over the building, as well as inside the MT-Based CHP system. And the types of data they can provide are as follows: temperature, humidity, gas/air/exhaust/liquid flow rate, electricity, current, building pressure, equipment status, and weather station data. Most of the sensors output a 4 to 20mA current, which has the advantage of avoiding signal attenuation over long wires. The current signal is converted into 0.88 to 4.4VDC voltage, with which the required data value is calculated through the HP VEE program and then recorded into the

computer. The data acquisition interval, which can be set by the user, is set to one minute.

3. Sensor Calibration

Sensor error is one of the main causes of measurement error. Appropriate periodic sensor calibration eliviates this problem to a large extent, besides appropriate data selection and processing.

For the calibration, a reference sensor is selected. The sensors that are to be calibrated are placed into the SDU chamber with the reference sensor, so that the radiation that they receive from the sun at the day time would be the same. The fan inside the unit is also turned on during the calibration process to provide air flow across the sensors, so that they will be able to face a same environment. . Ideally, all the sensors should have the same reading, while as a matter of fact, readings from each sensor deviate from the reading of the reference sensor, to some degree. The goal of the calibration is to write new calibration factors into the HP VEE system so that the readings of all the sensors are the same as the reading of the reference sensor, or, as close as they realistically can be.

During the calibration test, measurement data of these sensors will be collected for two days and then processed to be used in the calibration process. A quick way that we have been using to avoid the tedious calculation process is to use the curve-fitting feature in the MATLAB image toolbox. By plotting a Figure of all sensor readings vs. the reference sensor reading and doing linear curve fitting on all other sensor

readings, a form of $Y = B_0X + B_1$ can be derived for each sensor, where Y is the readings of the sensors to be calibrated and X is the readings of the reference sensor. Then, set $Y' = (Y - B_1)/ B_0 = X$ and write this new equation into the HP VEE system for each sensor as appropriate, all the sensors will then have the closest possible readings to those of the reference sensor when in the same environment.

With the calibration process above, measurements can be made more consistently.

A calibration sample of relative humidity sensors is shown in Figure 11. The deviation before calibration went up to 14% while the value after calibration is controlled within 4%.

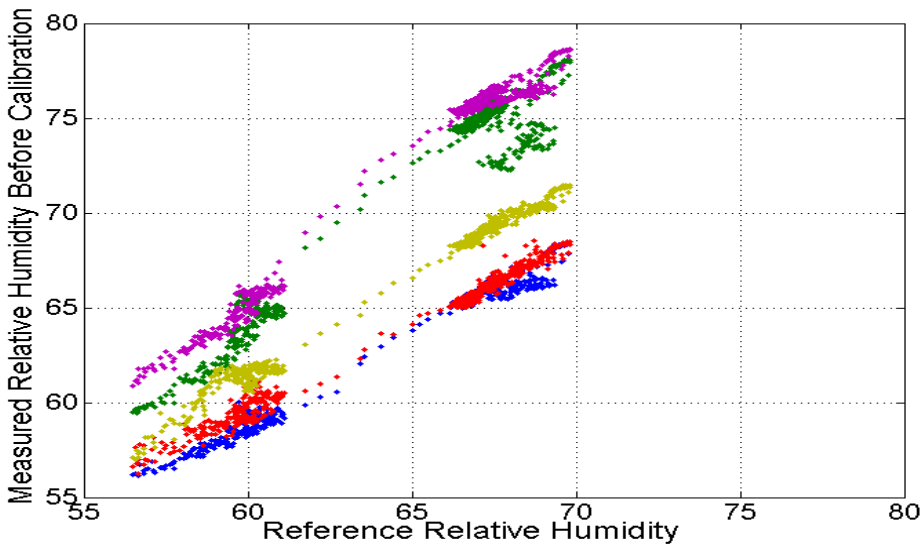

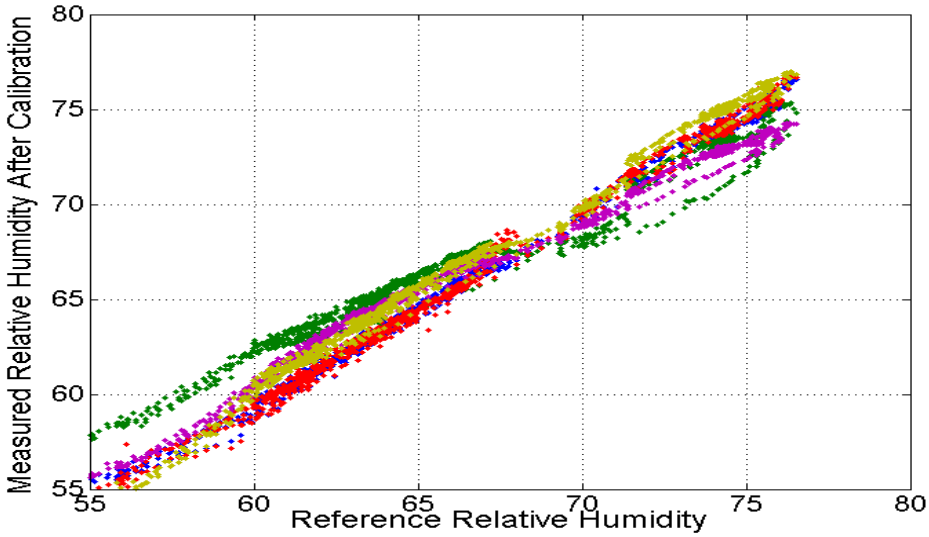

Figure 11 A Sample Calibration of Humidity Sensors

3 Motivation and Objectives

Motivation

The interests in CHP systems for building are growing rapidly nowadays, while many questions are to be solved and many improvements are yet to be done. The fuel flexibility, as well as the fast communication and in-time response between devices are both important topics in the CHP research work.

The fuel flexibility of CHP system is in fact the fuel flexibility of the power generation equipment. There are many other types of clean fuels, and each has its own advantages. The more flexible the CHP system is on fuel, the more opportunities there are for different applications.

The response time between prime mover (microturbine in our case) and thermally driven devices (absorption chiller in our case) is another problem. In cooling operations, the transient process is very important and cannot always be neglected. Especially for absorption cooling in CHP systems, it might require more than half an hour for the absorption chiller to reach its steady state, while it takes only a few minutes for the microturbine to stabilize its power output. What's more, the "steady state" is a relative description. The system reacts to state changes all the time, and the control devices then, would react to these changes to keep the system working as

expected. Hence, it's necessary to obtain a deeper understanding of the transient process, to which appropriate improvements related to control devices can be applied.

Much work has been done on simulating the steady state performance of absorption chillers with different simulation tools. [1]~[5] However, only a small effort has been put into the investigation of the transient characteristic of an absorption chiller, especially for chillers in CHP systems.

Objectives

The objectives of this study are:

1. Conduct an experimental performance evaluation of a CHP System in an occupied office building

2. Demonstrate CHP systems' fuel flexibility by running the microturbine on propane

    a) Convert the Microturbine fuel supply and pre-treat system

    b) Demonstrate the feasibility of running microturbine on propane, maintain stable operation

    c) Collect operating data

d) Compare the performance of the microturbine running on different fuels

3. Investigate the transient behavior of the absorption chiller by modeling its startup process.

4 Microturbine Fuel Flexibility

Overview and introduction

Microturbine

As the prime mover of a whole CHP System, a microturbine generates electric power for both the system and the building, and provides exhaust heat for the thermally driven units.

The key components of a microturbine, including the compressor, combustion chamber (or combustor), turbine, recuperator and generator, are as shown in Figure 12.

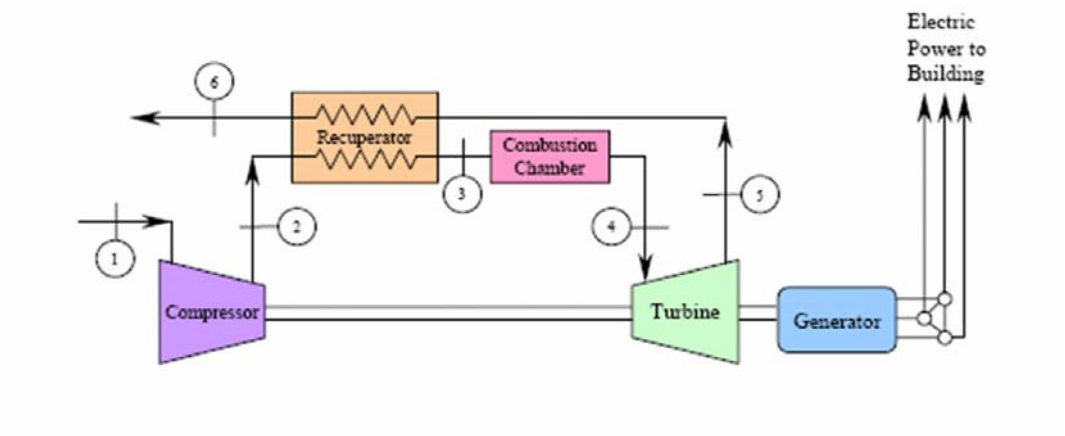

Figure 12 Schematic of Microturbine

Microturbine works on an improved Brayton Cycle, as shown in Figure13 below.

The cycle starts at state point 1, where the air is sucked into the compressor. The curve from 1 to 2 represents the polytropic compression of the air in the compressor. The air leaving the compressor is then heated in the recuperator, ideally, under a constant pressure. However, because of hydraulic resistance in the recuperator, a small pressure drop occurs during the heating process. Fuel and air is then mixed and ignited in the combustion chamber. 3 to 4 represents the combustion process. The high temperature combustion products, 4, enter the turbine to drive it for power production. 4 to 5 shows the polytropic expansion process in the turbine. Finally, from 5 to 6, the air leaves the turbine and enters the recuperator to provide heat for the incoming air before leaving the microturbine as exhaust air. This process in the recuperator would be under a constant pressure ideally, yet the hydraulic resistance again causes a small pressure drop during this process.

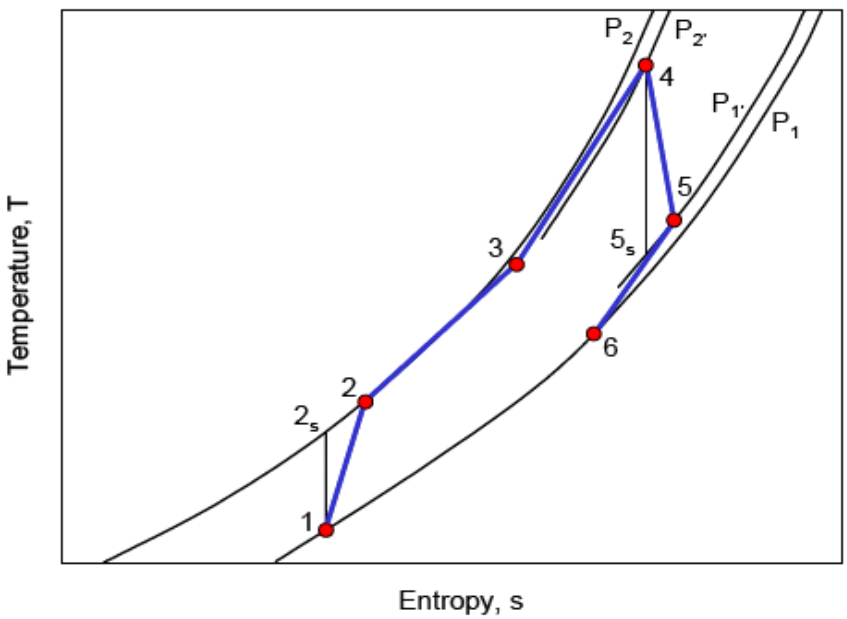

Figure13 T-S Diagram

Although operating on the same cycle, compared to a conventional gas turbine, microturbines have several advantages. They are lighter in weight and smaller in size. The measured emission levels of the fuel gas are very low, its NO_x emission rates can be less than 9 ppm, or less than 0.5 pounds per megawatt-hour (MWh). By contrast, the emission level from a typical power plant is 10 times higher[19]. So, microturbines have cleaner output and thus are environmentally green. As for fuels, they have multiple fuel capability, for example: natural gas, diesel, kerosene, propane, methanol and ethanol. With only one moving part, microturbines are expected to provide much greater reliability and a longer life cycle than conventional machines. An additional advantage is a low vibration rate. Although their power generation efficiency (~27%) is lower comparing to conventional power plant (30%~35%), the above advantages still make microturbines attractive.

The Microturbine in the MT-Based CHP System

The microturbine that is used in the MT-Based CHP system and studied here is designed for operating on natural gas exclusively and can provide up to 60 kW of power and 150 kW of heat for combined heat and power. It's an integrated system with controls and measurement systems.

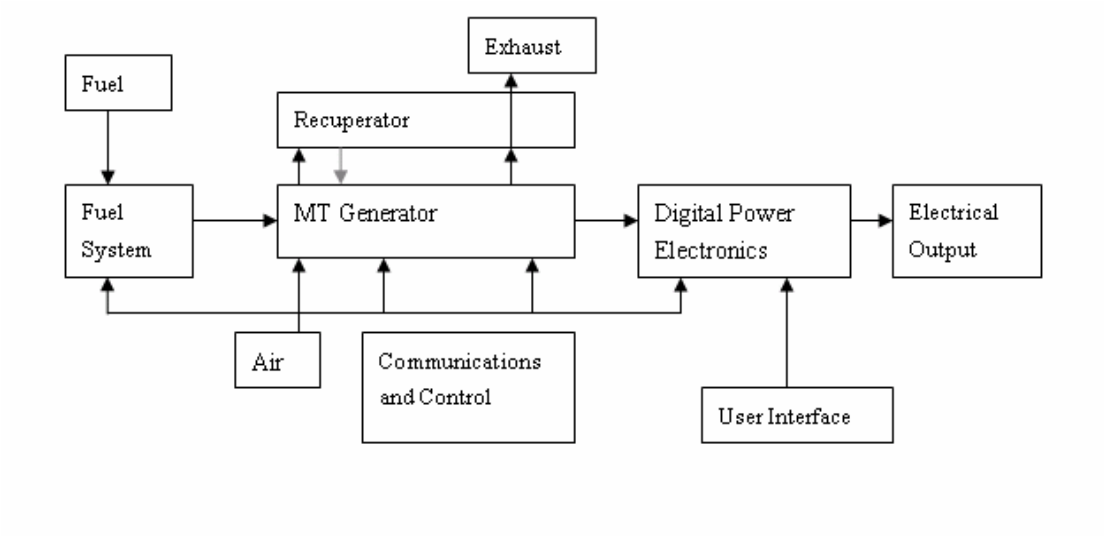

Figure 14 Schematic of the 60 kW Microtubine

The system incorporates a compressor, recuperator, combustor, turbine and permanent magnet generator; the key parts are shown in Figure 15. The rotating components are mounted on a single shaft that spins at up to 96,000 rpm, supported by air bearings. This is the only moving part of the microturbine. The generator is cooled by inlet air flow. The system uses no oil, lubricants, coolants or other hazardous materials, and has no pumps, gearbox or other mechanical parts.

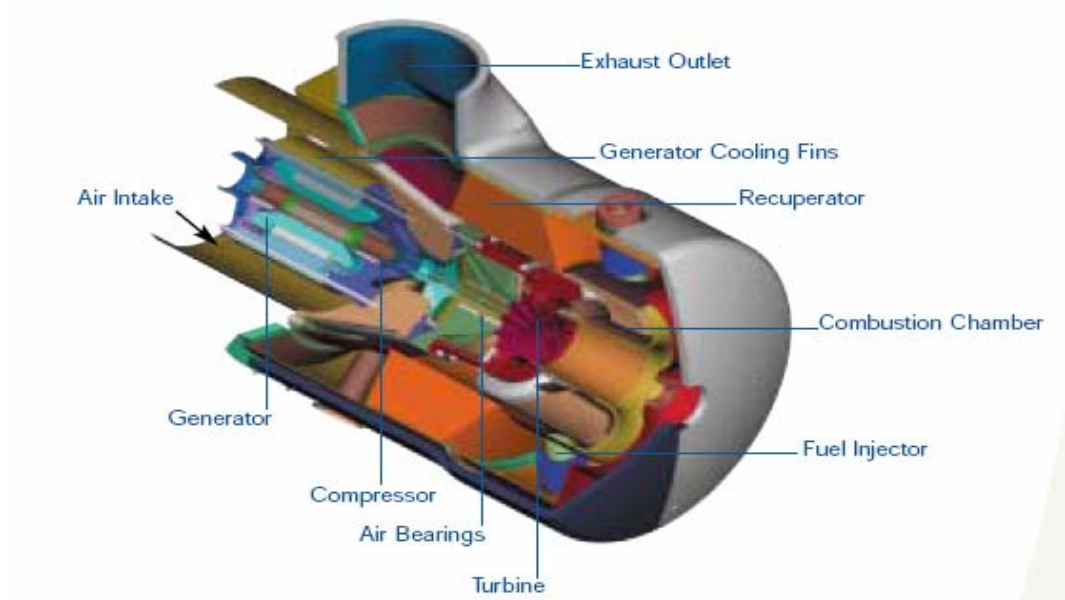

Figure 15 Microturbine Generator

The statepoints of the working cycle of the 60 kW MT are shown in Figure 16 .

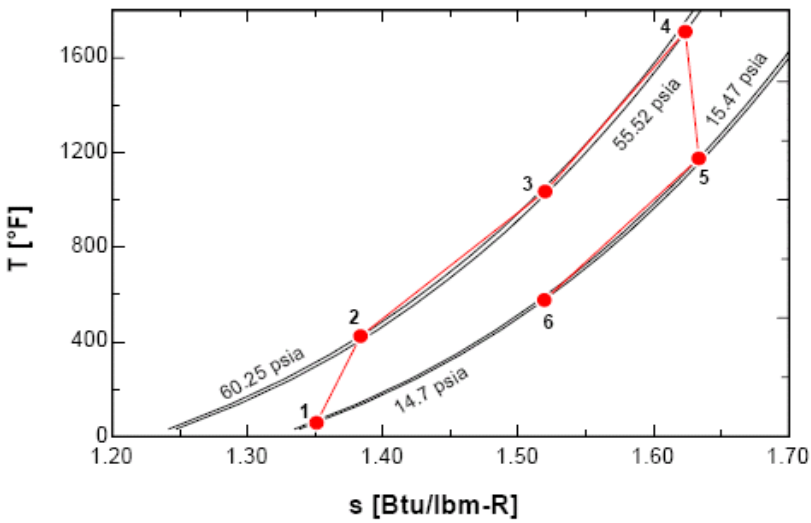

Figure 16 60 kW Microturbine Operating Statepoints

Figure 17 shows the thermal efficiency and power output as functions of ambient air temperature, provided by the manufacturer[19]. As can be seen on the graph, the output power can be kept constant at 60 kW until the ambient air reaches 86.7 °F, above which the output power drops linearly as the temperature rises. This is because the rotational speed of engine, which controls the volumetric air flow rate, has reached its maximum and cannot get any higher when the temperature goes above 86.7 °F. This causes the volumetric flow rate of air to stay constant, while the air density is reduced, which means the microturbine is actually taking in less air than the amount required for generating 60 kW electricity, so that the output power is reduced. The thermal efficiency degrades as the ambient temperature rises as well.

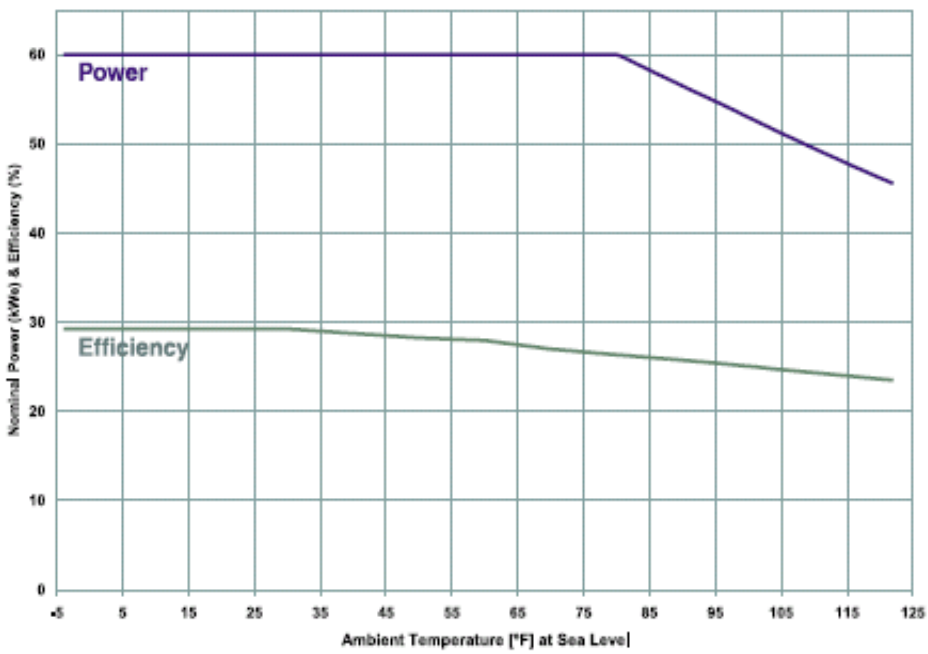

Figure 17 60 kW Microturbine Performance Comparison at Full Load

Numerous data of this microturbine have been collected through daily experiments as

well.

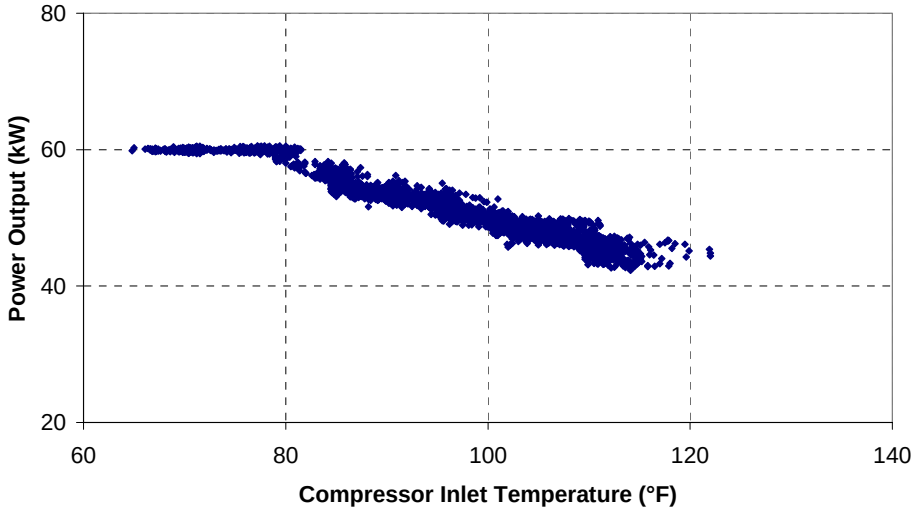

Figure 18 MT Power Output vs. Compressor Inlet Temperature

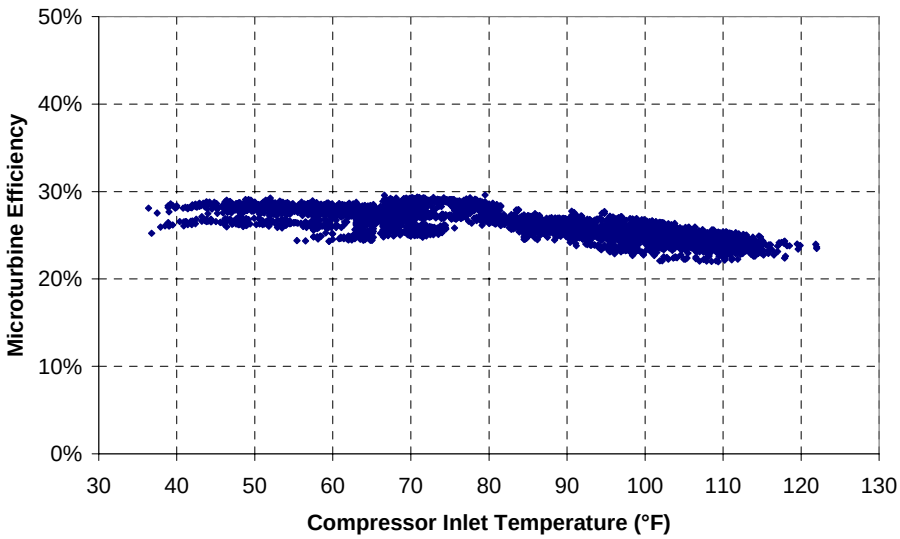

Figure 19 MT Efficiency vs. Compressor Inlet Temperature

Figure 18 and Figure 19 show the power output and electric efficiency of the MT vs.

compressor inlet temperature. And they are in accordance with information provided by the manufacturer.

The cause of power output and efficiency degradation can be validated from Figure 20.

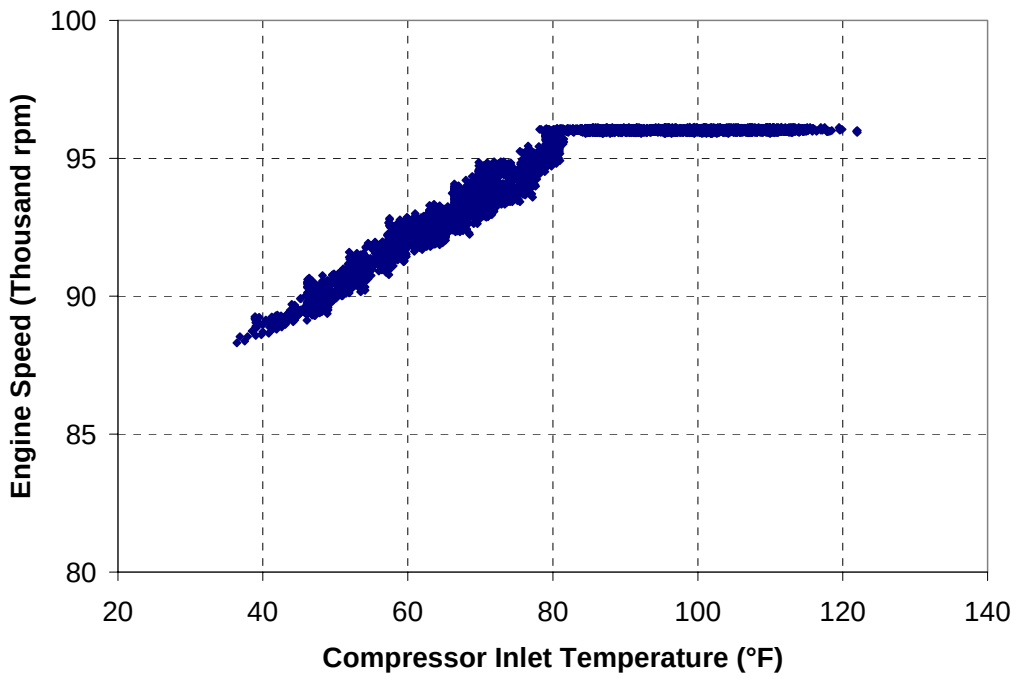

Figure 20 Engine Speed vs. Compressor Inlet T.

The engine speed rises as the inlet air temperature rises, until it reaches its limit, where the volumetric flow rate of the intake air reaches its limit too. As the temperature continues rising, the density of air decreases, resulting in reduced air intake, and thus power output and efficiency degradation.

Compressor inlet temperature is not exactly the ambient temperature; however, it relates to the ambient air temperature closely. The data collected showed a linear correlation between these two temperatures. This is caused by the fact that the ambient air is heated up by the exhaust gas due to the heat leakage from the engine core and the plenum box before entering the compressor.

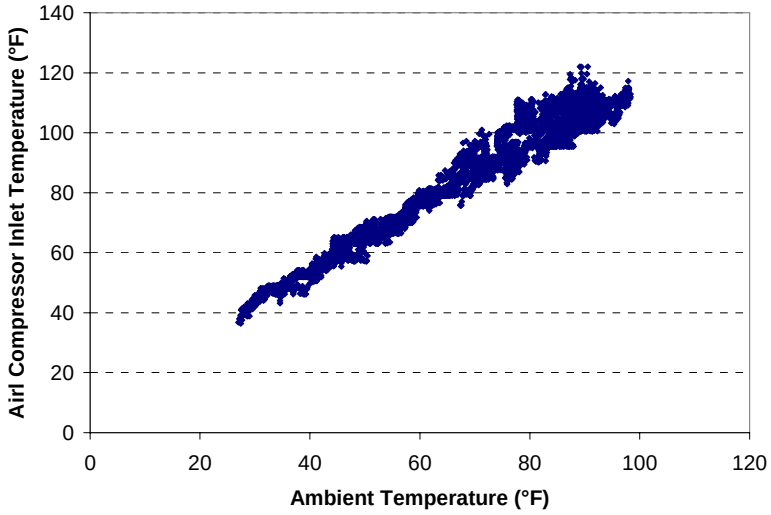

Figure 21 Compressor Inlet Temperature vs. Ambient Temperature

Properties of Fuels

Both natural gas and propane are clean fuels that contribute very low emissions to the environment.

Natural Gas

Natural gas is a fossil fuel source of energy, which represents more than one fifth of total energy consumption in the world. It has been the fastest growing fossil fuel since the seventies.

Natural gas is colourless, odourless, tasteless, shapeless and lighter than air. It is gaseous at any temperature over -161º C. When it is at its natural state, it is not possible to see or smell natural gas. For safety reasons, a chemical odorant that smells a little like rotten eggs, Mercaptan, is added to natural gas so that it can be smelled if there is a gas leak.

Natural gas is a mixture of light hydrocarbons including methane, ethane, propane, butanes and pentanes. Other compounds found in natural gas include CO_2, helium, hydrogen sulphide and nitrogen. The composition of natural gas is never constant, however, the primary component of natural gas is methane (typically, at least 90%), which has a simple hydrocarbon structure composed of one carbon atom and four hydrogen atoms (CH_4). So, usually, when calculating, methane's thermal property is used for natural gas. Methane is highly flammable, burns easily and almost

completely, while it emits very little air pollution. Natural gas is neither corrosive nor toxic, its ignition temperature is high, and it has a narrow flammability range, making it an inherently safe fossil fuel compared to other fuel sources. In addition, because of its specific gravity of 0.60, lower than that of air (1.00), natural gas rises if escaping, thus dissipating from the site of any leak.

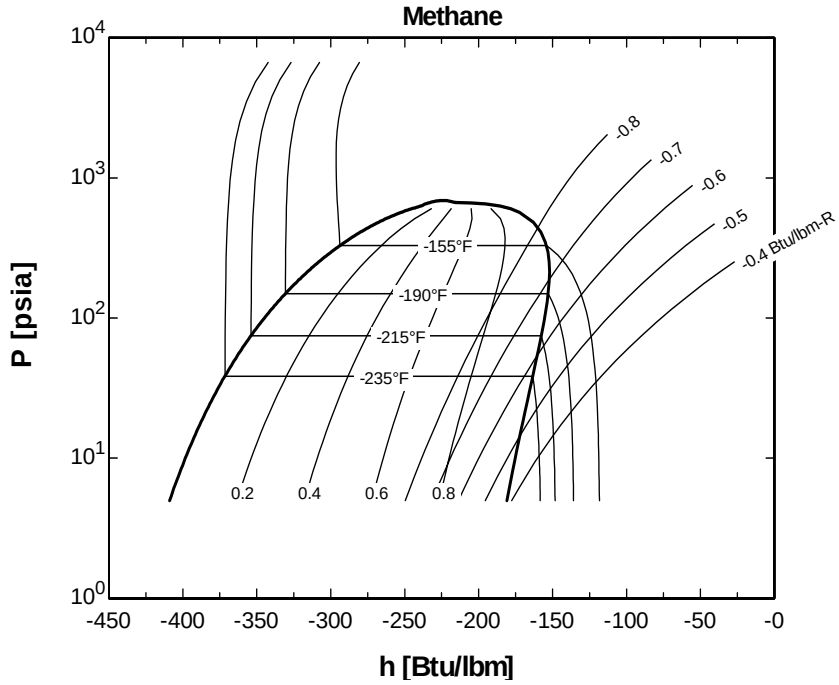

Figure 22 P-h Diagram of Methane

Propane

Propane is a liquefied petroleum gas and aromatic hydrocarbon that can be utilized as a gaseous fuel at relatively high ambient temperatures since it will vaporize at atmospheric pressure around –44°F. Propane is a heavy, colorless, flammable gas. Its chemical formula is C_3H_8. For use as a fuel, propane is liquefied under pressure and

sold in tanks, making it a very portable fuel source. The main advantage for using propane as fuel is that it has low pollution characteristics compared to other heavier fraction fuels and its higher energy density in comparison to other clean burning alternative fuels. The Lower Heating Value (LHV) of propane is about 46.4 MJ/kg, very similar to that of natural gas, which is 43 MJ/kg. The much higher density of propane as compared to natural gas results in much higher energy density per unit volume at the low pressures typical of gas delivery systems. While natural gas is difficult to store at a commercial or domestic site, propane's higher energy density makes storage less complicated.

Compared to natural gas, the saturation temperature of propane is much higher, for example: at 14.7psia, natural gas will evaporate/condense at - 258.7°F, while the saturation temperature of propane is - 43.6°F. When the propane pressure reaches 90 psig, which normally occurs at the place between microturbine and its fuel gas compressor, the saturation temperature can be 58°F, as in Figure 23. The 60 kW MT studied here has no warranty to run on propane currently, as condensation of propane in the delivery lines is one of the potential problems, this should be avoided by ensuring that a combination of high pressure and low temperature does not occur concurrently.

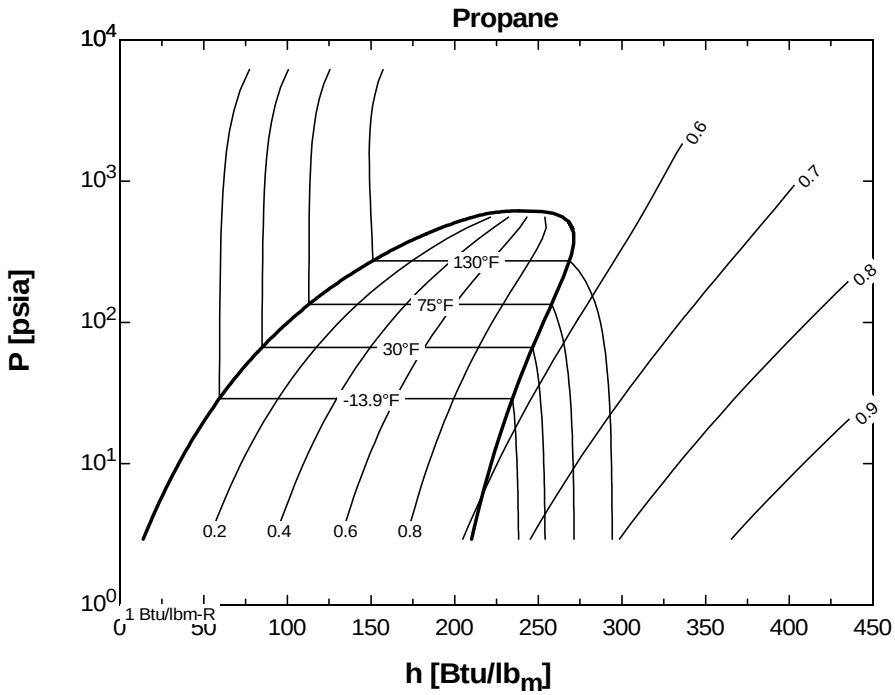

Figure 23 P-h Diagram of Propane

Comparison

Compared to natural gas, propane has the advantage of better compressibility so that it can be stored on site. The disadvantage of propane is that it cannot be operated under a pressure as high as natural gas, nor an ambient temperature as low as natural gas, due to the condensation concern.

<u>Experimental Setup</u>

Due to the property difference of these two types of fuel, different setups are required for the tests.

Natural Gas Test

The set up of the microturbine using natural gas follows the criteria from the manufacturer. The gas pressure is regulated at 0.2 psig at the gas meter, according to the set point of the gas company. The gas is then transported and filtered before entering the gas compressor, which is connected to the turbine to raise the pressure of the fuel to 90 psig. Gas pressure is regulated to 75 psig when being injected into the microturbine.

Propane Test

The 60 kW MT studied here is not designed for running with propane. Consequently it was necessary to take steps to protect the system before conducting the tests on propane.

The main concern is that, since the microturbine operates at a high speed (up to 96,000 rpm), any liquid on the turbine could cause damage to the engine. To do the test, several modifications were made to avoid liquid fuel condensation along the pipeline as a result of high pressure and/or low temperature. According to the manufacturer's requirements, it is important to maintain the gaseous fuel at 18°F above the dew point temperature throughout the fuel system.

Steps have been taken to keep the temperature high enough that no liquid propane enters the turbine.

A coalescing filter is installed to filter out liquid fuel, water and particulate matter, as shown in Figure 24 . It is located after the outlet of the compressor, just upstream of the microturbine where the highest pressure (90psig) exists in the system and condensed fluid is most likely to occur.

Figure 24 Coalescing Filter

Gas line pressure set points were also changed. In the first year of propane test, the gas pressure regulator after the compressor is set to 70 psig for propane (rather than natural gas's 75 psig) per the manufacturer's advice; and the regulator at the gas meter is set to 0.4 psig. Both regulators at the gas meter are as shown in Figure 25.

However, the low pressure settings of propane before the compressor caused several trips during the first year and resulted in some unsatisfying testing data in the first

year.

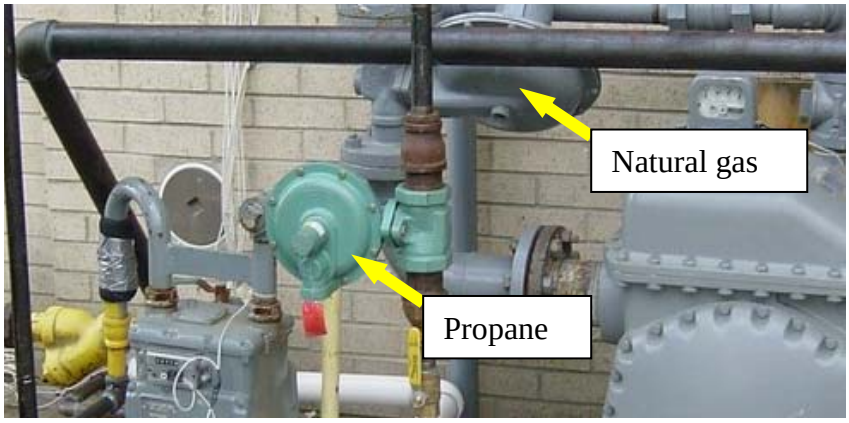

Figure 25 Natural Gas Regulator and Propane Regulator (Test year one)

In the second year of testing, a few more modifications were made on the pressure set points. The gas pressure at the inlet of the gas booster was changed to 10psig when the microturbine is idling and 8 psig when running; the regulator at the propane tank was set to 22~25 psig, as shown in Figure 26.

(a) Regulator#1 right after the propane tank set at 22~25 psig

(b) Regulator#2 before the compressor set at 10 psig

Figure 26 Regulators on the Pipeline (Test year two)

The gas line pressures for both years are shown in Figure 27.

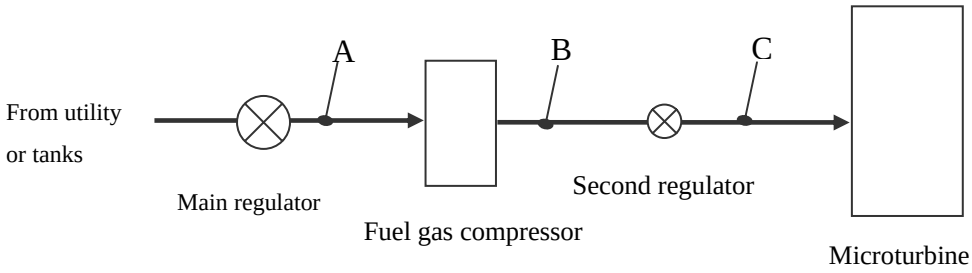

First year:

For natural gas:	For propane:
Point A – 0.2 psig	Point A – 0.4 psig
Point B – 90 psig	Point B – 90 psig
Point C – 75 psig	Point C – 70 psig

Second year

For natural gas:	For propane:
Point A – 0.2 psig	Point A – 10 psig/ 8 psig
Point B – 90 psig	Point B – 90 psig
Point C – 75 psig	Point C – 70 psig

Figure 27 Pressure Settings

In addition to pressure adjustments, temperature settings can be very important to avoid any condensation of the fuel along the pipeline. A heat trace was installed

along the pipeline with insulation to keep the fuel temperature between 80 and 120 °F.

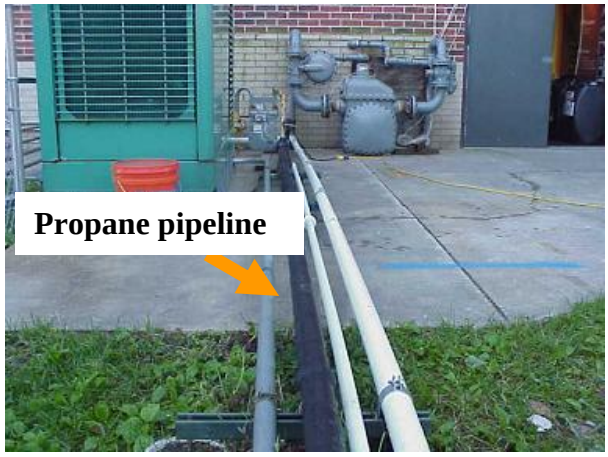

Figure 28 Propane Pipeline with Heat Trace and Insulation

Control software settings

The microturbine is operated through its remote control software provided by the manufacturer. This software is called a Remote Monitoring System and can be applied on both 60 kW MT and 30 kW MT, another type of microturbine manufactured by this company. Data points inside the MT can be monitored and recorded through this system, control of the MT is also completed by the software automatically. Users can also change the settings manually through it.

Since the 60 kW MT that is being tested is designed for natural gas only and had always been operating on it, fuel settings need to be adjusted before switching the machine to operating on propane.

Changes can be made through the fuel adjusting panel, as shown in Figure 29.

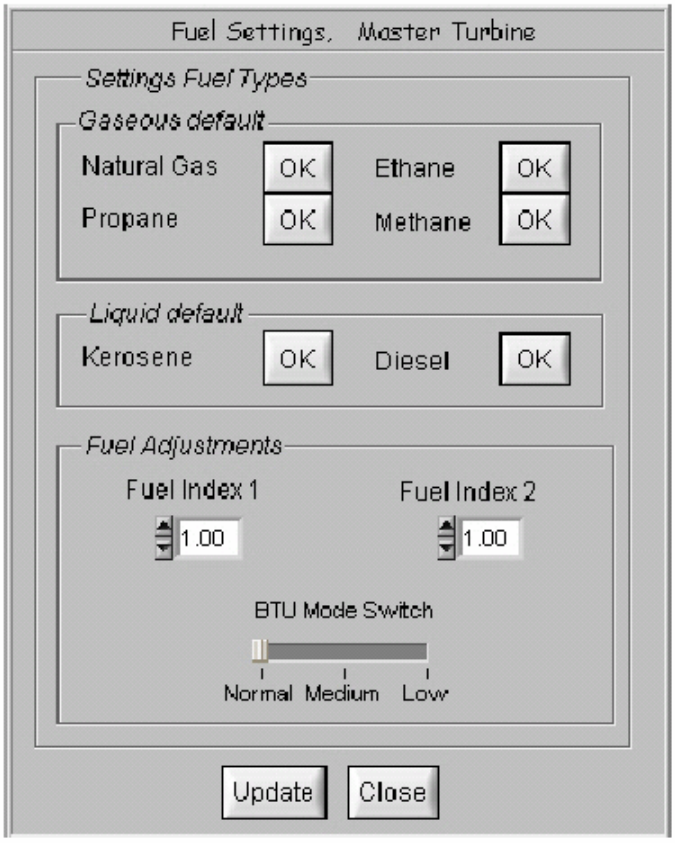

Figure 29 Fuel Setting Panel

This panel is used for both 30 kW MT and 60 kW MT, so the default fuels that are shown on the panel include all the fuels that can be used by either of these microturbines. If the fuel that is to be used is among the default fuels, adjustment can be completed by simply choosing the fuel on the panel. Otherwise, there are two "fuel indexes" that could be filled in by the user if a special fuel (e.g., a refinery byproduct) is used.

The BTU Mode Switch is to be set according to the higher heating value of the fuel,

the settings are:

- Normal = 970 – 2515 BTU/scf
- Medium = 700 – 970 BTU/scf
- Low = 350 – 700 BTU/scf

The purpose of this adjustment is to input the higher/lower heating value of the new fuel, so that the fuel control system can react correctly.

Data collection

Experimental data have been collected on a minute by minute basis through two different systems.

For data from the microturbine, the Remote Monitoring Software described in the previous section was used. By connecting the computer to the microturbine through an RS-232 serial cable, more than one hundred data points can be measured and recorded, including generator power output, net power output, compressor inlet temperature, turbine exit temperature, engine speed, etc. As for the data outside the microturbine (e.g. outdoor air temperature, fuel volumetric flow rate), they are measured by the HP VEE system described in Chapter Two.

The operations with both natural gas and propane were stable and reliable.

A comparison between the microturbine operating on natural gas and propane is

shown in Figure 30, with one typical day's data chosen for each fuel.

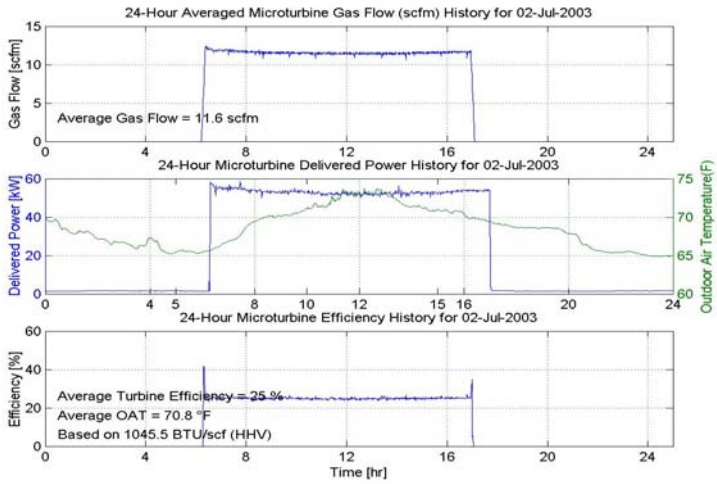

(a) on natural gas

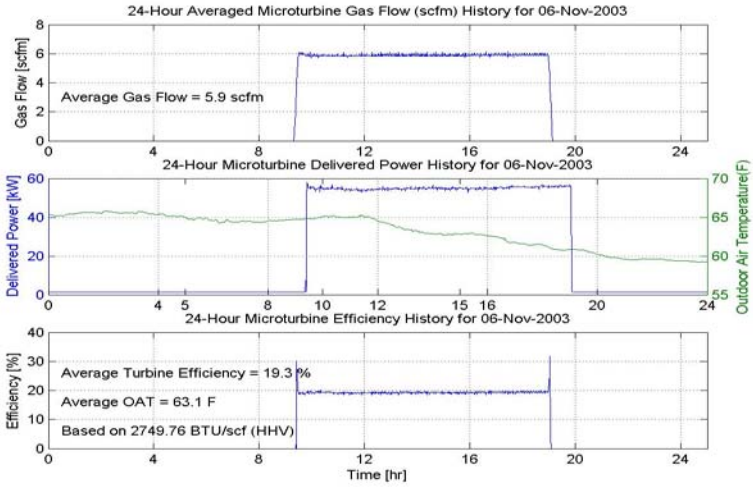

(b) on propane

Figure 30 MT Performance on Typical Days

<u>Data Processing</u>

To compare the microturbine's performance on both fuels in detail, all the data acquired through experiments have been exported to Excel Sheets for further evaluation.

Fuel flow rate

The volumetric fuel flow rate is measured on a minute-by-minute basis. Due to concern over possible measurement errors, a ten-minute rolling average was used in the analysis.

Unit Volume Conversion

To be in accordance with the manufacturer's calculation, for the natural gas, an LHV of 950 btu/scf is used; and for propane, an LHV of 2286 btu/scf is used. These two values are both reference numbers under standard conditions, yet the volumetric flow rates were measured under the pressure at the gas meter at the ambient temperature. Thus, to calculate the actual heat input by these two fuels, a conversion from unit volume under operating condition to unit volume under standard condition has been made, so that the input heat would be more accurate.

Two EES programs have been written to calculate the corresponding volumetric flow rate under standard conditions for both fuels. By inputting the ambient temperatures obtained minute-by-minute during the experiment, a conversion factor between the measured volumetric flow rate and the ones under standard conditions for both fuels

at each minute can be derived and used for further processing.

Initial Calculation

Initially, two criteria were used to evaluate the performance of the two fuels.

The first one is the net output power at full load plotted vs. compressor inlet temperature. The result is plotted in Figure 31, it can be observed that the net electric power output of the MT degrades when compressor inlet temperature increases, yet there is no obvious difference in power output from running on either fuel.

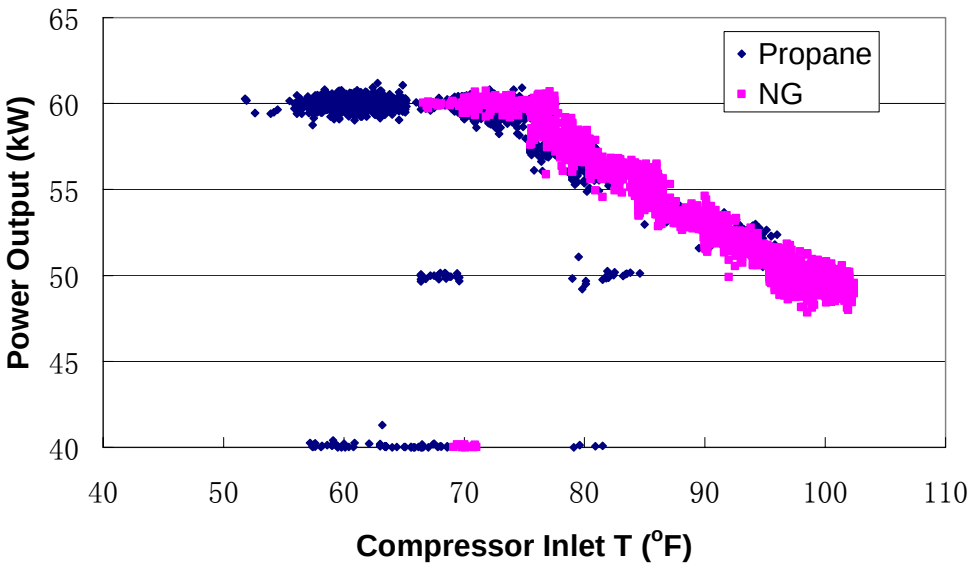

Figure 31 Power Output vs. Compressor Inlet Temperature

The second criterion is net efficiency. This is another parameter to evaluate the performance of each fuel; calculations have been done using the equation described

below:

$$\text{Net efficiency} = \frac{\text{MT net output power}}{\text{LHV} \times \text{Volumetric flow rate} \times \text{Conversion factor}} \times 100\%$$

However, as shown on Figure 32, microturbine net efficiency was lower when running on propane.

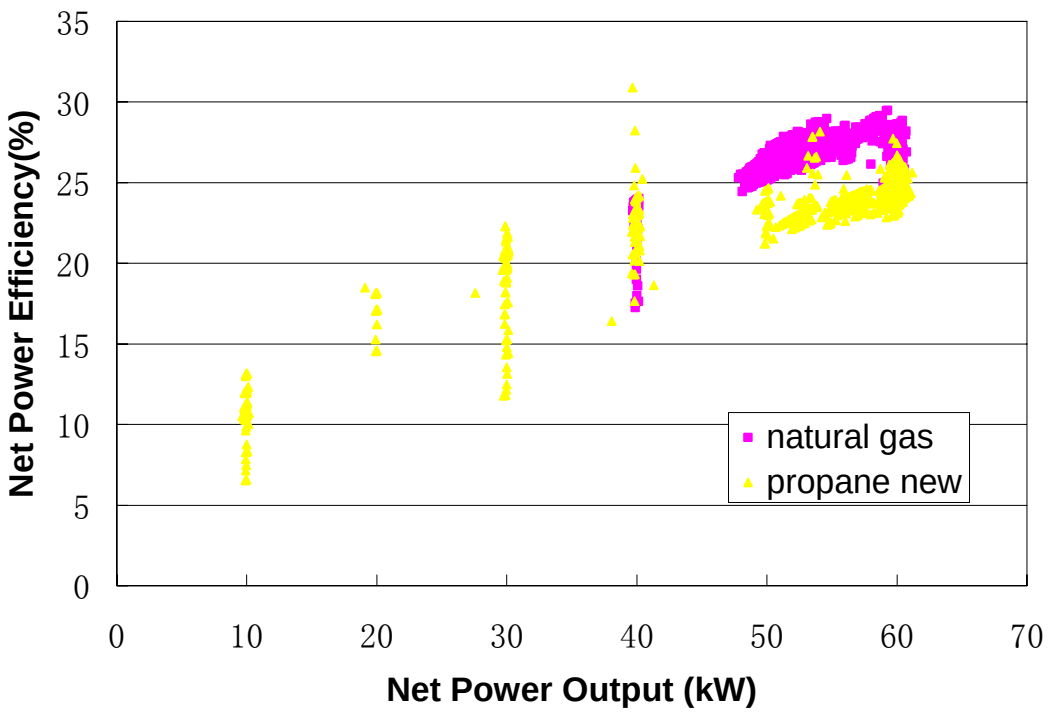

Figure 32 MT Net Power Efficiency Comparison

Theoretically, these two types of fuel should have the same efficiency; this has been proved on the 30 kW MT, another type of microturbine manufactured by the same company that is capable of running on both natural gas and propane. The reasons why the efficiency is lower when the 60 kW MT is operating on natural gas are not

intuitively obvious.

A first possible contributing factor to be investigated here is the parasitic power consumption, meaning that the design of this microturbine itself caused the efficiency difference since the 60 kW MT is not designed for natural gas.

Since the MT powers itself while running, the parasitic power consumption is the first thing to check. The design difference could be causing more parasitic power consumption since it was not intended for use with propane.

The parasitic power is defined and calculated as below:

parasitic power = gross output power – net output power

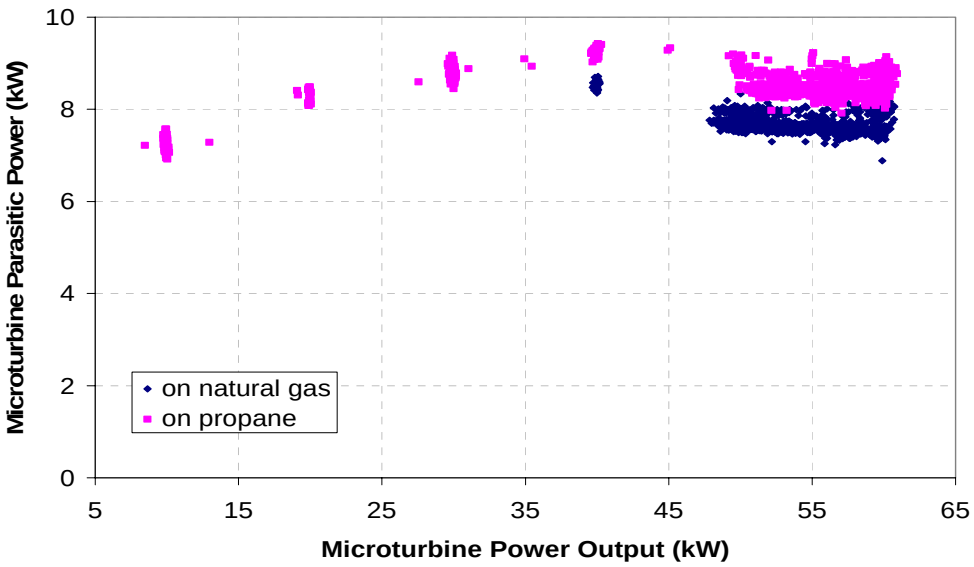

Figure 33 MT Parasitic Power Consumption Comparison

As shown in Figure 33, running on propane consumes more parasitic power than when running on natural gas when the output power is reaching the full capacity, as has been assumed above. Most of the parasitic power is consumed by the compressor. Since the fuel gas compressor is designed exclusively for natural gas, it is possible that it consumes more power when compressing propane. Hence the parasitic power evaluation focused largely on the fuel gas compressor.

The MT produces the same amount of net power whether burning natural gas or propane. Since propane consumes more parasitic power as shown in Figure 33, the MT should be producing more gross power when running on propane. If the gross output power efficiencies on both fuels are the same, we can conclude that the parasitic power difference is one of the primary causes of the efficiency difference.

To figure out whether the assumption above is true, the gross power efficiencies of both fuels have been calculated.

The gross power efficiency is defined and calculated as below:

$$\text{Gross MT efficiency} = \frac{\text{MT gross output power}}{\text{LHV} \times \text{Volumetric flow rate} \times \text{Conversion factor}} \times 100\%$$

However, as is shown in

Figure 34, the difference in gross power output efficiency between the two fuels is comparable to the difference in net efficiency. Hence we conclude that differences

in parasitic power cannot be a primary cause of the efficiency difference.

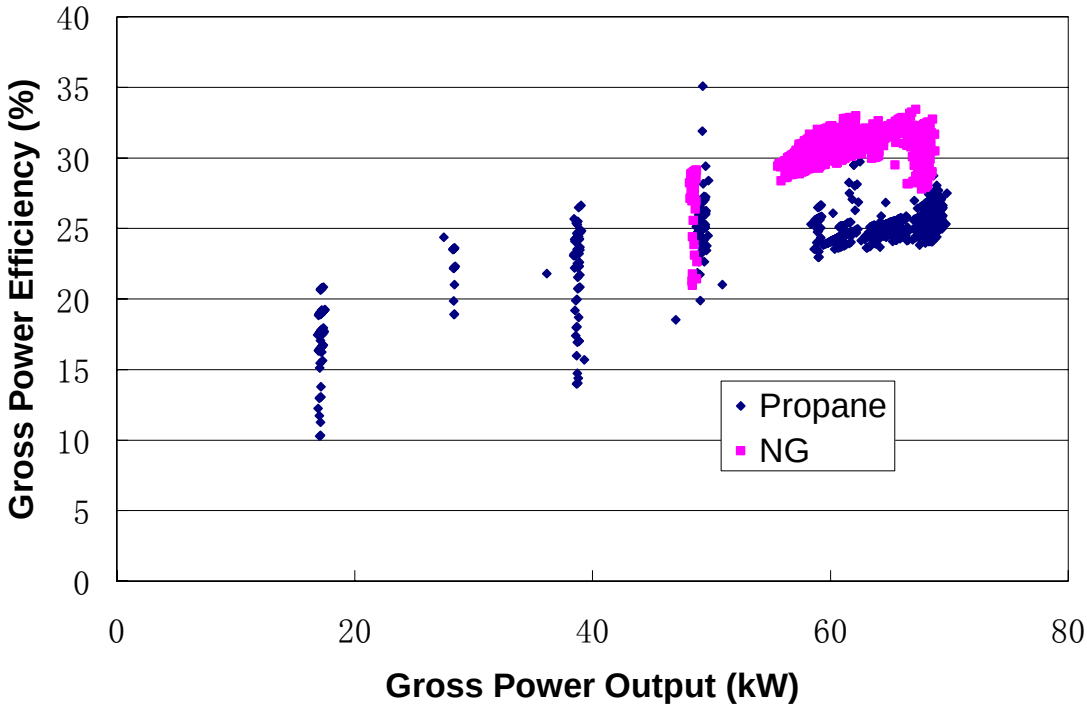

Figure 34 Efficiency of Gross Power Comparison

Further Analysis of Efficiency Degradation

Since parasitic power has been proven not to be the main cause for the efficiency degradation, further analysis is needed.

The 30 kW MT is designed to run on both natural gas and propane, and has a similar efficiency when operating on both fuels. It is helpful to compare these two different types of microturbine to find out the difference, which could probably be the reason

for the performance efficiency degradation.

Fuel Control Analysis

When switching the fuel, the only change that the operator makes is to the fuel settings, which is done on the Fuel Setting Panel shown in Figure 29. The microturbine then automatically adjusts itself for the new fuel. The changes in control logic are based on the 30 kW MT operating parameters because the 60 kW MT is intended for operation on natural gas only. For this reason and the fact that the two microturbines operate at different pressures, the control logic was considered to be a potential cause of the efficiency difference.

1. Similar Aspects

For both 30 kW and 60 kW microturbines, the intake gas flow rate is controlled by a device called smart proportional valve (SPV) in the fuel system. The SPV regulates the intake gas volumetric flow rate so that the MT runs at the desired engine speed and turbine exit temperature.

To work with different fuels, the fuel type has to be set in the fuel device control panel in the Remote Monitoring System, as discussed in Chapter 3. By doing this, the fuel control device would identify the higher heating value of the fuel and adjust the SPV accordingly to control the volumetric flow rate.

Because both types of microturbines share the same control software, their fuel

control devices work on the same strategy. That is, the ratio of the volumetric flow rate of propane to that of the natural gas is the same for both units. Note that propane operating parameters programmed into the Remote Monitoring Syestem are based on 30 kW MT operating conditions and do not include an adjustment for the 60 kW MT's operating conditions in the propane control parameters.

2. Different Aspects Comparison

The biggest difference between these two microturbines, in terms of the fuel system, is the gas intake pressure at the SPV.

The recommended intake pressures of natural gas and propane for the 30 kW MT are 55 psig and 45 psig respectively, while those recommended for the 60 kW MT are 75 psig and 70 psig.

Since the two systems require different gas intake pressures, the gas going into the 30 kW MT has a different density and density ratio from the gas going into the 60 kW MT. This indicates that, although the 60 kW MT maintains the same volumetric flow rate ratio when operating on propane, the mass flow rate ratio might not necessarily be the same. A simple calculation is shown below:

When the ambient temperature is 55 °F, natural gas has a density of 3.274 kg/m^3 at 55 psig and 4.226 kg/m^3 at 75 psig; propane has a density of 8.296 kg/m^3 at 45 psig and 12.28 kg/m^3 at 70 psig. It can be calculated that the intake gas density ratio between propane and natural gas is 2.534 of the 30 kW MT, and 2.906 of the 60

kW MT. With the same volumetric flow rate ratio and higher density ratio, the 60 kW MT has a higher mass flow rate ratio between propane and natural gas, which could result in C60 taking in more propane than expected.

As stated previously, natural gas and propane have similar lower heating values based on unit mass. Thus, to input the same amount of heat, the mass flow rate between propane and natural gas should be 1.0126. So, when the 60 kW MT is running on propane, it takes in more gas than it needs to; and this would result in a lower electric efficiency.

Gas Mass Flow Rate of the 60 kW MT

An EES program has been written for this calculation and analysis.

Firstly, the density of natural gas under 0.2 psig (gas pressure at the meter) and 75 psig (gas pressure before entering the MT, where the SPV comes into play); the density of propane under 8 psig (gas pressure at the meter) and 70 psig (gas pressure before entering the MT) have been calculated. With the gas density at the meter and volumetric flow rate measured, the mass flow rate of the 60 kW MT of each fuel is calculated and shown as below in Figure 35.

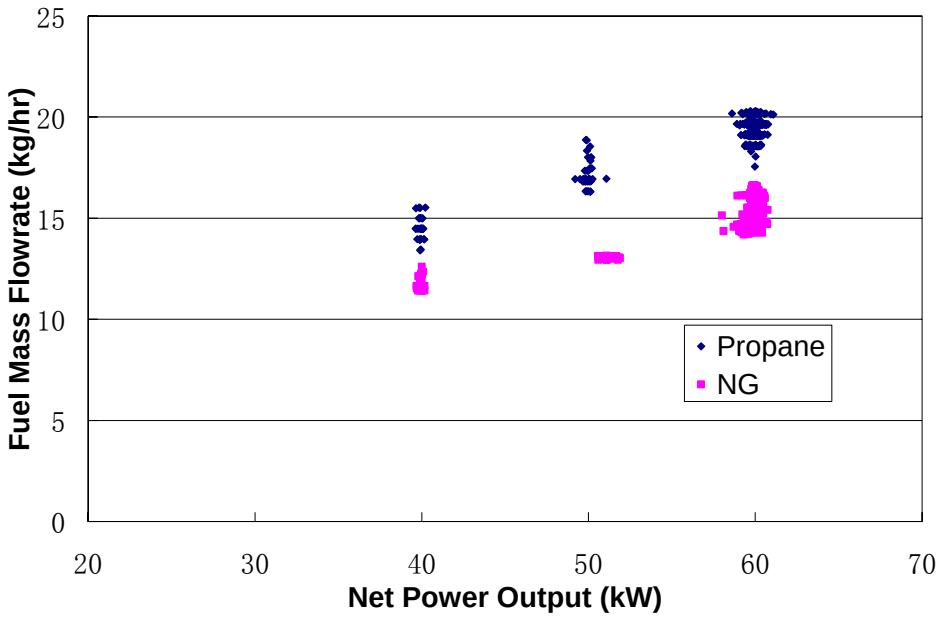

Figure 35 Mass Flow Rate Comparison

As can be seen, propane always has a higher mass flow rate than natural gas and thus provides more heat input to the microturbine and results in lower efficiency. As speculated above, the gap of mass flow rate between the two fuels becomes larger when the power output grows, resulting from the growing discrepancy between the volumetric flow rates. Since the LHV of these two fuels based on unit mass are close to each other, a larger mass flow rate indicates larger heat input. When producing the same amount of electric power, the one with larger heat input will have lower electric efficiency unless that additional heat can be converted to power. Although the microturbine actually takes in more heat when it is running on propane, it ejects the excessive heat as long as it reaches the power output demand and operates safely.

Now, the next question to be solved is, how much does the mass flow rate ratio

influence the efficiency ratio?

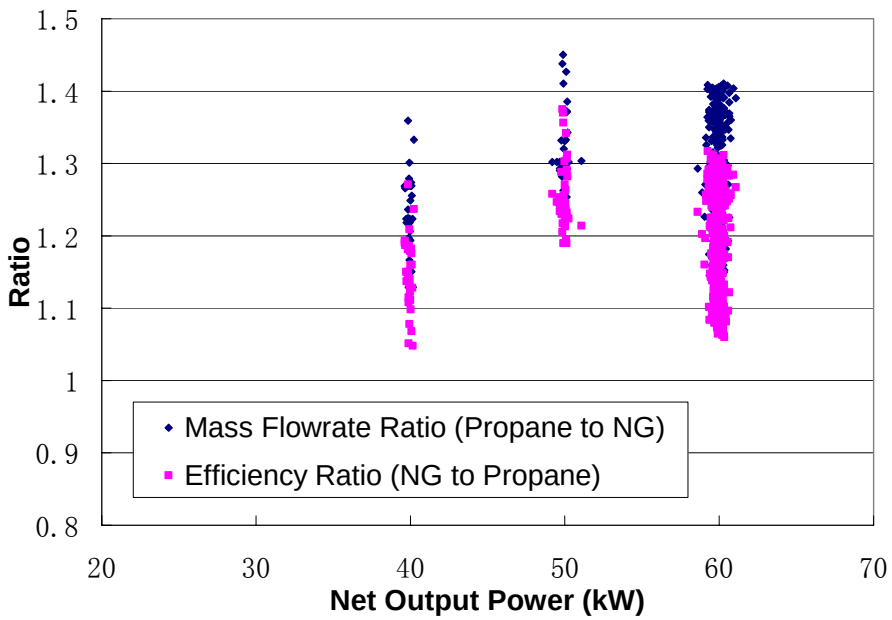

Figure 36 Ratios Comparison

The answer can be found in Figure 36. This plot shows the mass flow rate ratio between propane and natural gas; as well as the efficiency ratio between natural gas and propane. The two ratios show good agreement, indicating that the mass flow input is actually the main reason causing the efficiency degradation.

30 kW MT Calculation

Keeping the above result in mind, a series of calculations is done for the 30 kW MT. Since detailed operating data of the 30 kW MT is not available to us, we are assuming that these two types of fuels are operating on the 30 kW MT with the same volumetric

flow rate ratio as the 60 kW MT at the inlet of the microturbine.

The volumetric flow rate ratio of the 60 kW MT before the SPV is calculated through an EES program. The density ratio between the propane (at 70 psig) and natural gas (at 75 psig) at their corresponding ambient air temperatures are obtained by calculating in EES program. By dividing the mass flow rate ratio that has already been calculated by this density ratio, the volumetric flow rate ratio at the inlet of the microturbine is derived.

The density ratio between propane and natural gas at the inlet of the 30 kW MT is calculated in a similar way as it has been done for the 60 kW MT. The density of propane is calculated at 45 psig, and that of natural gas at 55 psig.

Apply the volumetric flow rate ratio obtained from the operation of 60 kW MT and the density ratio calculated under the gas intake condition of 30 kW MT, a mass flow rate ratio assuming that these two fuels are operating on the 30 kW MT is derived.

Figure 37 illustrates the difference in mass flow ratios and the efficiency ratio between the 30 kW and 60 kW microturbines. It can be observed that the mass flow rate ratio on the 30 kW MT is lower than that on the 60 kW MT.

This result further verifies the speculation made above, that the 30 kW MT, while the fuel control device operates the same way as it dose on the 60 kW MT, is taking in less propane. In other words, the 60 kW MT is taking in more of propane than the fuel control device meant to for a certain power output, thus having a larger amount of

heat input, and resulting in efficiency degradation.

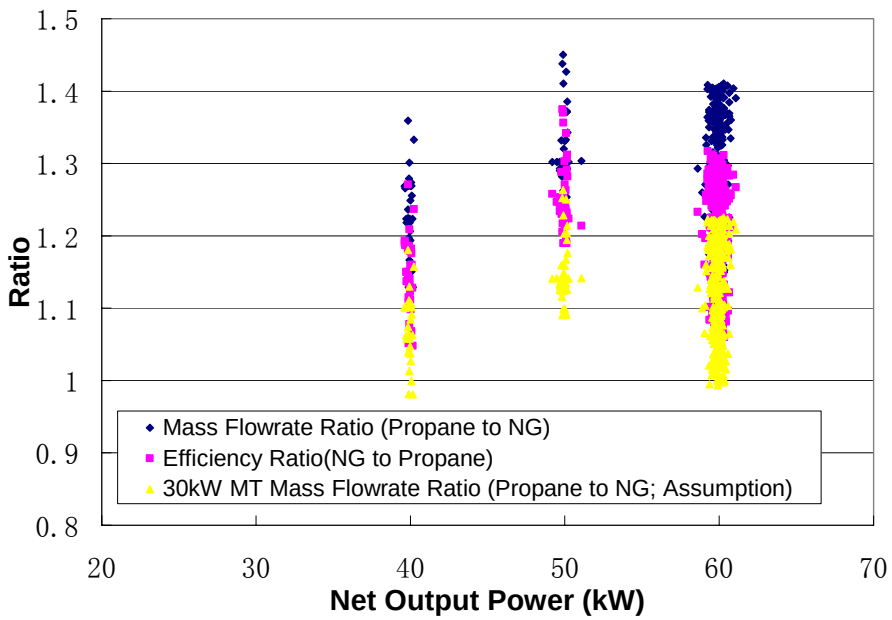

Figure 37 Ratio Comparison w/ 30 kW MTAssumption

With the above calculation and comparisons, conclusions can be made.

The efficiency reduction that occurs when the 60 kW MT is running on propane is mainly caused by the fuel control device. Because it is programmed for the 30 kW MT, another model that this company manufactures, which runs on both natural gas and propane, and has different inlet gas pressures from the 60 kW MT, the fuel control device doesn't fit the 60 kW MT. While the density of both fuels change due to the inlet pressure change, the fuel control device still maintains the volumetric flow rate ratio that was defined for the 30 kW MT operation, so that the 60 kW MT takes in more fuel than it needs which results in efficiency reduction.

To correct the efficiency reduction problem on the 60 kW MT, one of the following steps is suggested.

1. Reprogram fuel control device, make it suitable for the fuel inlet pressure of the 60 kW MT.

2. Manually change the HHV value for propane in the fuel control panel, make it higher than the default value so that the fuel control device will take in less amount of propane than it is now.

However, the efficiency of the microturbine is not everything in a CHP system, since the system utilizes the exhaust heat to drive its thermally driven equipment, the exhaust heat that is provided by the microturbine is also an important topic for discussion.

Exhaust Heat Analysis

Observation

While the 60 kW MT runs at lower efficiency on propane than it does on natural gas, an interesting and important fact that should be considered is that with lower efficiency, running on propane can actually provide more exhaust heat.

Figure 38 and Table 3 show the comparison of average heat input and exhaust heat

output of the 60 kW MT between running on natural gas and propane. Running on propane produces a larger amount of exhaust heat than natural gas, due to its larger heat input.

Power Demand (kW)	Propane			Natural Gas		
	Heat Input (kW)	Exhaust Heat (kW)	Gross Power Output (kW)	Heat Input (kW)	Exhaust Heat (kW)	Gross Power Output (kW)
60	267.7	199.2	68.5	223.7	156.0	67.7
50	232.6	173.2	59.4	191.7	133.9	57.8
40	192.9	143.6	49	172.1	124.1	48

Table 3 Average Heat Input and Exhaust Output Summary

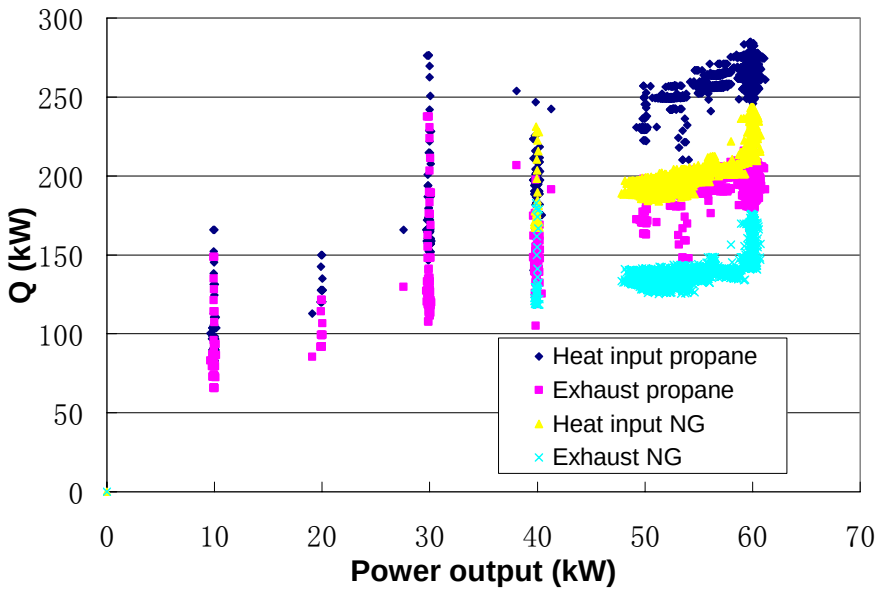

Figure 38 Comparison of the Amounts of Waste Heat

While from a power generation point of view, more exhaust heat output is meaningless and a total waste of energy, it is not exactly the same for a CHP system.

Exhaust Heat for Building Cooling

As introduced earlier, a CHP System works in a way that utilizes the waste heat generated in the process of power generation. For different systems, the demands of power and heat differ from each other. From this point of view, electric power output efficiency should not be the only criterion to evaluate the electric generation equipment's performance in a CHP System, since higher electric power generation efficiency doesn't necessarily indicate higher total efficiency of the system.

In a CHP System that requires high heat/power ratio, a lower efficiency actually helps. Taking the microturbine that we are studying for example, it has a higher electric power output efficiency when operating on natural gas than when operating on propane, which is better for the microturbine's performance. However, as shown in

Figure 38, the exhaust heat provided by the microturbine when operating on natural gas on full power is about 150 kW, which means it could only drive the thermally driven units that require heat input of 150 kW or less. In the meantime, when operating on propane, the exhaust heat output could reach up to 200 kW, and would therefore be capable of driving the thermally driven machines that require heat input up to this value, which could not be done when operating on natural gas.

From this viewpoint, while satisfying the same demand for electric power, using

propane can provide more exhaust heat, allowing larger thermally driven machines to be included in the overall system. That may result in a higher total efficiency for the overall system.

If we take a closer look from the building loads' point of view, as a matter of fact, when applying BCHP systems to a certain building, the ideal case would be that the building has a uniform demand ratio between power/heating/cooling throughout the year (e.g. Figure 39), so that no adjustment will need to be made and the system can run year round to obtain more savings.

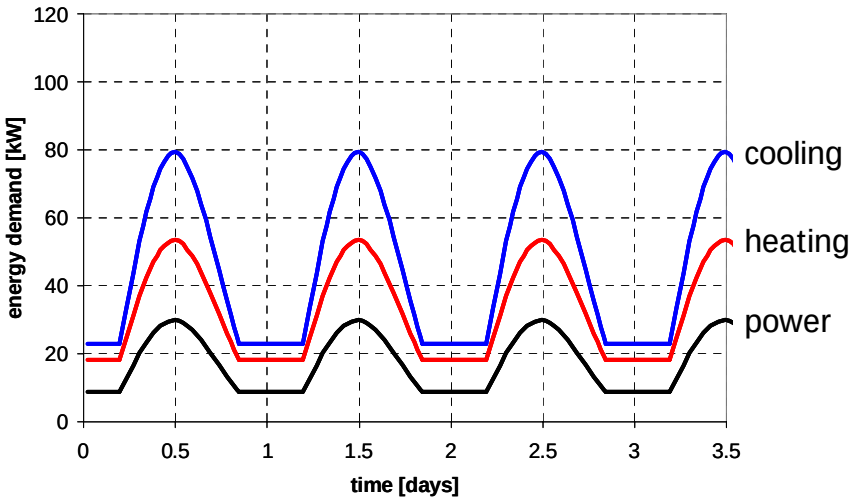

Figure 39 Idealized Load Profiles for Cooling Heating and Power[11]

However, in real situations, demands of the buildings vary a lot throughout the year, as can be seen in Figure 40 and Figure 41.

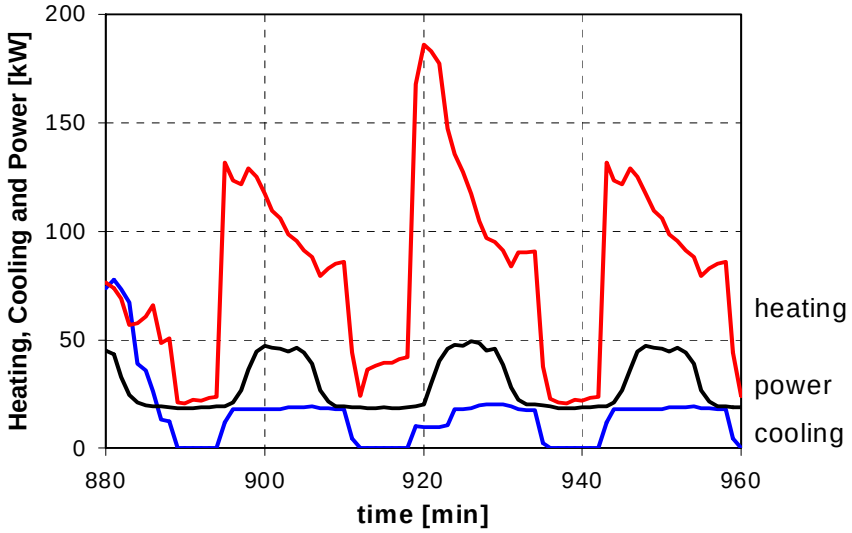

Figure 40 Real Building Load Profile (heating season)[11]

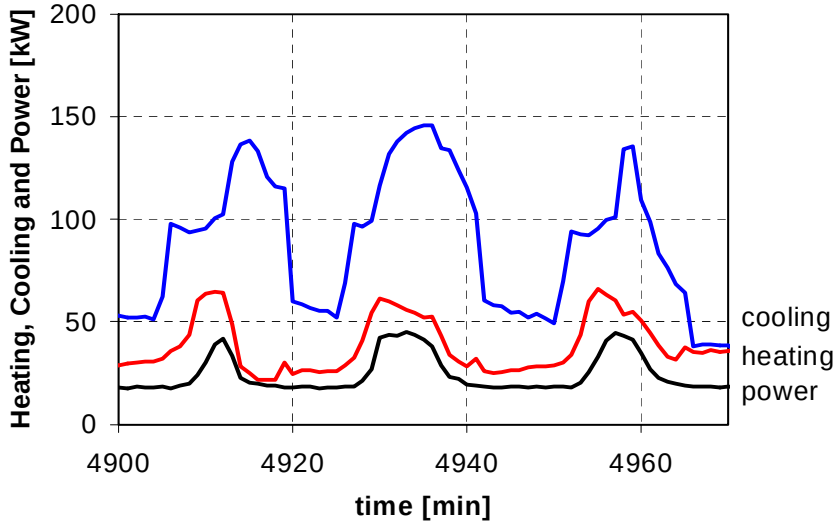

Figure 41 Real Building Load (cooling season)[11]

While the power demand remains comparatively constant, both the heating and cooling demand vary in different seasons. With a system which can only provide power and exhaust heat on a constant ratio, when the heating/cooling demand goes up, the operator has two choices. First, increase the power output of the system to

generate more heat. If this is chosen, more electric power is produced, reverse power to the grid might happen, and the system might be shut off. The other method would be to not change anything and keep the system running without interruption, but the increased heating/cooling demand has to be satisfied somehow.

Suggestions

To be able to satisfy the varying demand without confronting problems, a system that outputs constant electric power while varying its exhaust output flexibly to meet the heating/cooling load would be very helpful.

With the exhaust heat profile calculated and shown above in

Figure 38, the idea of adjusting heat output while maintaining constant electric power output seems to be possible.

The initial suggestion that could be made from the calculation and the plot above would be that we could adjust the fuel supply to adjust the exhaust heat output. For example, manually adjusting the fuel setting to increase the fuel supply to more than required for the power output, so that the excess will be released in the form of exhaust heat and more exhaust can be obtained.

With that in mind, a CHP system can be developed to meet the varying heating/cooling load while keeping a constant power output. The idea is, designing a power generation device for a CHP system whose power output is set to meet the

basic electric power demand of the building. And make its lowest heat generation, that is, the exhaust heat output when operating on the highest power generation efficiency, able to meet the basic heating/cooling demand of the building. Then, during operation, according to the variation of the heating/cooling load, adjust the amount of fuel intake to decrease the power generation efficiency, while keeping a constant power output level.

To make a CHP system as described above possible, new control devices are needed to be developed to be able to adjust not only for the fuel type, but also for the exhaust heat demand. Another challenge to be solved is to figure out the fuel supply range that can be used for the machine, so that it doesn’t take in more fuel than it can handle.

5 Absorption Chiller Transient Model

Introduction to absorption technology and absorption chiller

As one of the thermally powered units in the system, the absorption chiller utilizes the exhaust heat from the MT to provide cooling to the building.

Compared with traditional vapor-compression systems, the essential difference between those systems and absorption systems is that the absorption system converts heat of a given temperature to heat of another temperature without any intermediate use of work [13]. The solubility difference of certain chemicals in water under different temperature and pressure conditions is employed to produces water vapor, which is then used to provide cooling capacity.

Early equipment used a mixture of ammonia and water as an absorption working pair, ammonia as the refrigerant and water as the absorbent. This pair is still in use today in a range of applications. However, because of the toxicity of ammonia, it is often restricted to applications in which the equipment is outdoors to allow natural dilution of any leaks. After 1945, another working pair, Lithium Bromide (LiBr)-Water started to be used widely. In this pair, however, water serves as the refrigerant while the Lithium Bromide / water solution is the absorbent. LiBr absorption machines account for approximately 5% of the U.S. commercial cooling market and as much as

50% of the markets in Japan, Korea, and China[21].

Figure 42 shows a schematic of a single effect absorption cycle, with LiBr-Water as the working pair.

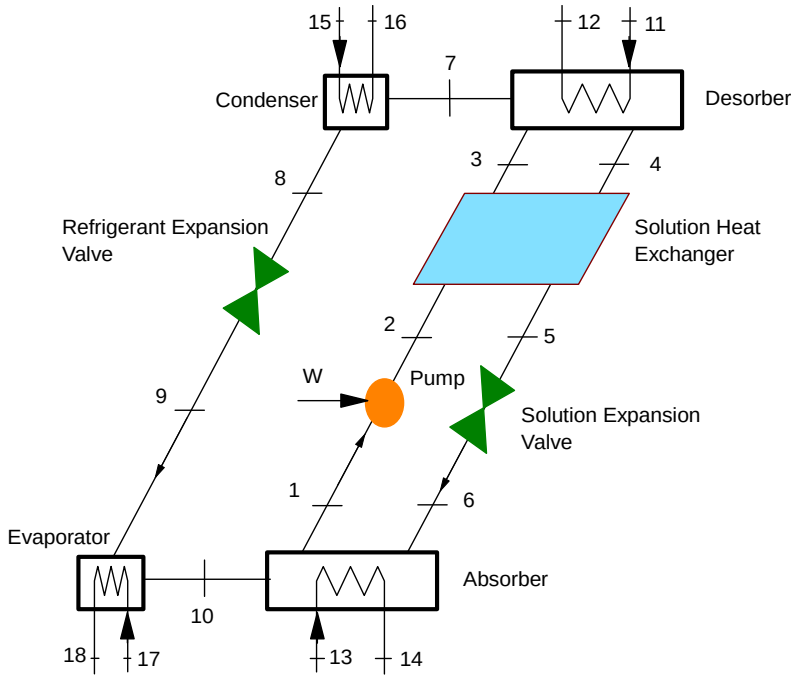

Figure 42 Diagram of Single Effect Absorption Chiller

The working cycle can be described as below. Although LiBr is the absorbent, solution poor in LiBr is usually defined as weak solution, while solution rich in LiBr is usually defined as strong solution. This definition is also used here.

For absorbent (LiBr solution) circulation:

1 Weak solution comes out of absorber

1-2 Weak solution is pumped into the solution heat exchanger

2-3 Weak solution flows through the solution heat exchanger

3-4 Weak solution is heated in the desorber, becomes strong solution by releasing water, and flows out of the desorber

4-5 Strong solution flows through the solution heat exchanger, rejecting heat to the weak solution

5-6 Strong solution is expanded through solution expansion valve

6 Strong solution goes into the absorber

For refrigerant (water) circulation:

3-7 Water is released from the weak solution and becomes vapor

7-8 Vapor condenses in the condenser

8-9 Water is expanded by the refrigerant expansion valve

9-10 Water evaporates in the evaporator, provides cooling

10 Vapor enters into the absorber, where it is absorbed into the weak solution

For external fluid:

11-12 Exhaust gas/ heat resource flows through the desorber, ejects heat into the desorber

13-14 Cooling water flows through absorber

15-16 Cooling water flows through condenser

17-18 Chilled water flows through evaporator

The chiller is operated under two different pressure stages. The desorber and condenser operate under the high pressure, which is determined by both the condensation pressure in the condenser and the saturation pressure of the strong solution in the desorber; while the absorber and evaporator operate under the low pressure, which is determined by the evaporation pressure in the evaporator, as well as the saturation pressure of the weak solution in the absorber.

Absorption Chiller in the MT-Based CHP System

The absorption chiller being used in this CHP system is a single effect LiBr absorption chiller.

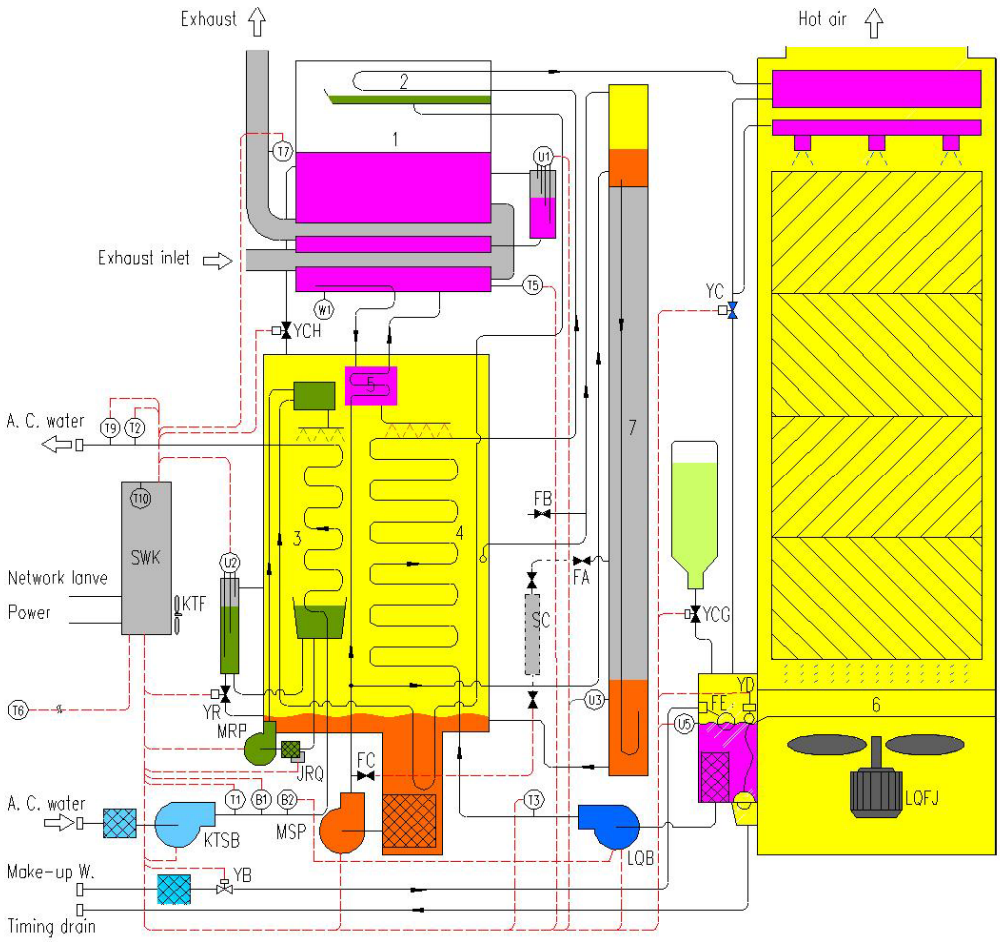

Figure 43 Schematic of the Single Effect Chiller[29]

The chiller, as described earlier, is connected with the MT through the exhaust gas duct, and is driven by the exhaust heat. The heat recovery loop is shown below in Figure 44. The dampers are used to control the amount of the exhaust gas that flows through the duct and that be ejected to the ambient air. It adjusts according to the cooling demand of the chiller. When the cooling demand increases, the damper adjusts to the direction which allows the intake of the exhaust gas to increase; while it

moves to the opposite direction to decrease the amount of exhaust gas flowing to the chiller as the cooling demand drops. There is always some ambient air provided through the fans to mix with the exhaust gas since the chiller cannot stand the temperature of the exhaust gas.

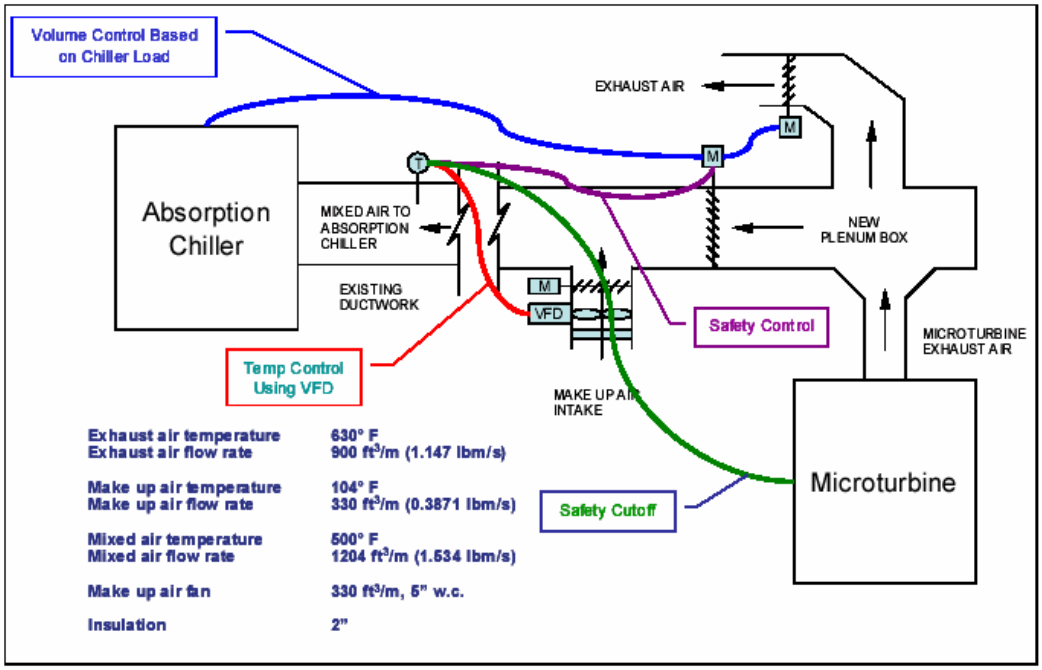

Figure 44 Exhaust Heat Management and Safety Control of the MT-Based CHP System

As stated previously, the MT reaches its steady states very fast (~ 5 minutes) while the chiller does it slowly (~ 1 hour). To be able to get a clearer idea of how the chiller performs during its transient process, in order to develop a better control strategy, a transient model has been built.

Model Description

Assumptions

To create a dynamic model of the absorption chiller, several assumptions have been made, as listed below:

1. The solution leaving the absorber (point 1) is saturated.
2. The enthalpy change across the pump is very small and can be omitted.
3. Perfectly insulated components.
4. The temperature of the vapor generated (T_7) equals the average temperature of the entering (T_3) and leaving (T_4) temperature of the solution from which it's generated.
5. No superheating in the evaporator, nor subcooling in the condenser.
6. The water (point 9) entering the evaporator is saturated.
7. Isenthalpic expansions.
8. The strong solution entering the absorber is saturated.
9. There's a certain amount of solution storage in the absorber.
10. The pump reaches steady state flow rate quickly (negligible startup period)

and maintains a constant rate.

11. No reverse mass flow from condenser to generator.

12. Valves are treated ideally such that there's no time delay. .

Modeling of Components

The chiller is composed of five major components (heat exchangers): solution heat exchanger, desorber, condenser, evaporator and absorber. Based on the operation principle and characteristics, the model of the chiller is first described as three different parts: solution heat exchanger, desorber & condenser, absorber & evaporator. The integration of the components and the simulation of the absorption chiller will be addressed in the next section.

There are two different families with regard to the devices that are modeled: lumped parameter models and distributed parameter models. As for heat exchanger models, the former method treats each heat exchanger as a single control volume, and calculates heat transfer using the empirical UA; while the latter one splits the model into several nodes and solves the equations numerically. For our model, the lumped parameter model is chosen since the outlet conditions of each component are of the greatest interest here.

1, Solution Heat Exchanger

Solution heat exchanger is the component in which the weak solution pumped up from the absorber and the strong solution flowing out from the desorber exchange their energy, as shown in Figure 45.

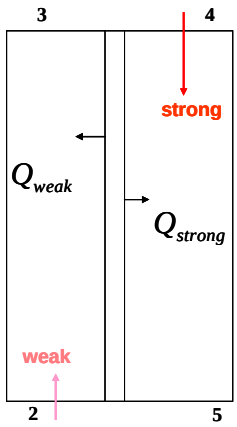

Figure 45 Schematic of Solution Heat Exchanger

The energy balance of both solution streams are described by the equations below[14]:

$$T_3 = T_{hx} - (T_{hx} - T_2)\exp(-\frac{UA_{hx_w}}{\dot{m}_3 \cdot Cp_w}) \quad (1)$$

$$\dot{Q}_{hx_w} = \dot{m}_3 \cdot Cp_w \cdot (T_3 - T_2) \quad (2)$$

$$T_5 = T_{hx} + (T_4 - T_{hx})\exp(-\frac{UA_{hx_s}}{\dot{m}_4 \cdot Cp_w}) \quad (3)$$

$$\dot{Q}_{hx_s} = \dot{m}_4 \cdot Cp_s \cdot (T_4 - T_5) \tag{4}$$

The temperature change of the solution heat exchanger itself is calculated by

$$Cp_{hx} \cdot M_{hx} \cdot \frac{dT_{hx}}{dt} = \dot{Q}_{hx_s} - \dot{Q}_{hx_w} \tag{5}$$

2, Desorber & Condenser

The desorber and condenser work together as a pair, sharing the same pressure: the high stage pressure of the chiller. The vapor that is generated in the desorber flows into the condenser and is then condensed. The condensing pressure corresponding to the condensing temperature in the condenser determines the high stage pressure. Meanwhile, this pressure is also constrained by the saturation pressure of the strong solution in the desorber. Thus, at every time step, a new equilibrium pressure that works for both containers is calculated.

For the desorber, it's assumed that it adjusts the outflow of solution to maintain a certain amount of solution (m_{st}), and the solution stored has the same state as the strong solution exiting.

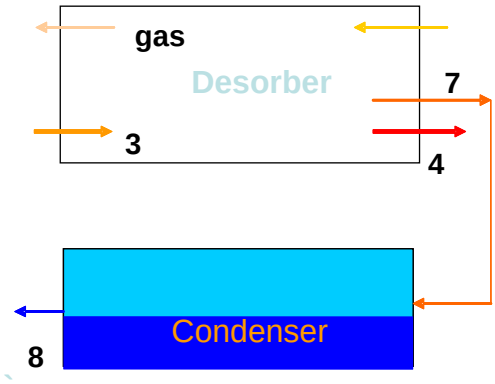

Figure 46 Schematic of Desorber/Condenser Pair

The mass and species balance of the solution flowing through the desorber are

$$\dot{m}_3 = \frac{dm_{st}}{dt} + \dot{m}_4 + \dot{m}_7 \tag{6}$$

where $\dot{m}_3$ is the mass flow rate of weak solution flowing into the desorber, m_{st} is the solution stored in the desorber, $\dot{m}_4$ and $\dot{m}_7$ are the mass low rates of the strong solution and water vapor flowing out of the desorber respectively.

$$\dot{m}_3 \cdot x_3 = (\dot{m}_4 + m_{st}) \cdot x_4 \tag{7}$$

where x_3 is the concentration of weak solution and x_4 is the concentration of strong solution.

The heat transferred from the hot metal of desorber to the solution that flows through it can be described with an LMTD heat transfer equation:

$$\dot{Q}_{d_in} = UA_{d_in} \cdot LMTD_d \tag{8}$$

where $LMTD_d = \dfrac{T_4 - T_3}{\ln\left(\dfrac{T_d - T_3}{T_d - T_4}\right)}$, T_3 is the temperature of the weak solution flowing into the desorber, T_4 is the temperature of the strong solution flowing out of the desorber, and T_d is the temperature of the desorber metal.

The solution absorbs the heat, becomes stronger, and generates water vapor. The energy change happens during this process is the same as the heat that is transferred from the metal into the solution; and can be expressed by:

$$\dot{Q}_{d_in} = \Sigma \dot{m}_k \cdot h_k = (\dot{m}_4 + m_{st}) \cdot h_4 + \dot{m}_7 \cdot h_7 - m_{st} \cdot h_{st} - \dot{m}_3 \cdot h_3 \tag{9}$$

where h_3, h_4 and h_7 are the enthalpy of weak solution, strong solution, and water vapor respectively, and h_{st} is the enthalpy of the solution stored in the desorber, which is in fact the h_4 from the last time step.

The heat transfer between the metal of the desorber and the solution in the desorber is balanced with the energy change of the solution, and can be expressed as:

$$\dot{Q}_{d_in} = UA_{d_in} \cdot LMTD_d = \Sigma \dot{m}_k \cdot h_k \tag{10}$$

The energy and heat transfer balance of the exhaust gas is:

$$T_{12} = T_{11} + (T_{des} - T_{11}) \exp(-\frac{UA_{d_out}}{\dot{m}_{11} \cdot Cp_{gas}}) \tag{11}$$

$$\dot{Q}_{d_out} = Cp_{gas} \cdot \dot{m}_{11} \cdot (T_{11} - T_{12}) \tag{12}$$

The temperature change of the desorber can be calculated as:

$$Cp_d \cdot M_d \cdot \frac{dT_d}{dt} = \dot{Q}_{d_out} - \dot{Q}_{d_in} \tag{13}$$

For the condenser, the energy balances on the vapor side and the cooling water side are:

$$\dot{Q}_{c_in} = \dot{m}_7 \cdot (h_7 - h_8) = UA_{c_in} \cdot (T_8 - T_c) \tag{14}$$

$$T_{16} = T_{15} + (T_c - T_{15}) \exp(-\frac{UA_{c_out}}{\dot{m}_{15} \cdot Cp_{water}}) \tag{15}$$

$$\dot{Q}_{c_out} = \dot{m}_{15} \cdot Cp_{water} \cdot \left(T_{16} - T_{15}\right) \tag{16}$$

The temperature change of the condenser metal can be calculated as:

$$Cp_c \cdot M_c \cdot \frac{dT_c}{dt} = \dot{Q}_{c_in} - \dot{Q}_{c_out} \tag{17}$$

Coupled with the property routines for water and aqueous LiBr solution, the above

equations are solved simultaneously as a set at every time step.

3, Evaporator & Absorber

Similar to the previous pair, the evaporator and absorber work together. The condensed water, after isenthalpic expansion at the expansion valve, evaporates in the evaporator, and then flows into the absorber, where it would be mixed with the strong solution coming back and rejects heat.

The low stage pressure of the chiller exists in these two components and is determined by both the evaporation pressure and the saturation pressure of the solution inside the absorber. And the value of this pressure is solved for at every time step as well, in a way similar to the method applied to the desorber & condenser pair.

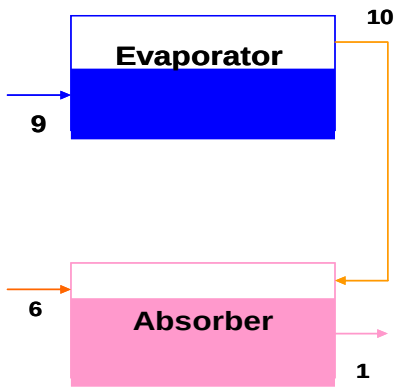

Figure 47 Schematic of Evaporator & Absorber

For the evaporator, from the evaporation temperature, the vapor enthalpy is calculated, and the energy and heat transfer balance at the water vapor side can be written as:

$$\dot{Q}_{e_in} = \dot{m}_7 \cdot (h_{10} - h_9) = UA_{e_in} \cdot (T_e - T_9) \tag{18}$$

And, the calculation of the cooling water side is done with the equations below:

$$T_{18} = T_{17} + (T_e - T_{17}) \exp(-\frac{UA_{e_out}}{\dot{m}_{17} \cdot Cp_{water}}) \tag{19}$$

$$\dot{Q}_{e_out} = \dot{m}_{17} \cdot Cp_{water} \cdot \left(T_{17} - T_{18}\right) \tag{20}$$

The temperature change of the evaporator can be calculated as:

$$Cp_e \cdot M_e \cdot \frac{dT_e}{dt} = \dot{Q}_{e_out} - \dot{Q}_{e_in} \tag{21}$$

For the absorber, the energy of the mass storage in it is also taken into account. Since the solution leaving the absorber is assumed to be at constant mass flow rate, which is relatively small compared with the solution storage, only the energy balance equation is adopted here. Similar to the desorber and condenser pair, it is expressed as:

$$\dot{Q}_{a_in} = \Sigma \dot{m}_k \cdot h_k = UA_{a_in} \cdot LMTD_a \tag{22}$$

where $$LMTD_a = \frac{T_6 - T_1}{\ln\left(\frac{T_6 - T_a}{T_1 - T_a}\right)}$$

The energy balance on the cooling water side is written as

$$T_{14} = T_{13} + (T_{abs} - T_{13}) \exp(-\frac{UA_{a_out}}{\dot{m}_{13} \cdot Cp_{water}}) \tag{23}$$

$$Q_{a_out} = \dot{m}_{13} \cdot Cp_{water} \cdot \left(T_{14} - T_{13}\right) \tag{24}$$

And the temperature change of the absorber can be calculated as:

$$Cp_a \cdot M_a \cdot \frac{dT_a}{dt} = \dot{Q}_{a_in} - \dot{Q}_{a_out} \tag{25}$$

This set of equations, similar to the desorber & condenser pair's, is coupled with the properties routine, being solved simultaneously at every time step.

Integration of Components Models

Following the flow direction of the solution/refrigerant, the outputs of one component would be the inputs of the next one. The simulations of each component are thus connected. In the mean time, the outputs of each time step serve as the input of the next one.

Modeling Tool

The simulation is completed in MATLAB Simulink®. An ODE 45 solver and a relative tolerance as 1e-5 are chosen. The time step is set as variable with a minimum time step of 0.5 seconds.

Simulink Blocks

A Simulink block consists of a set of inputs, a set of states, and a set of outputs where the outputs are a function of the sample time, the inputs, and the block's states.

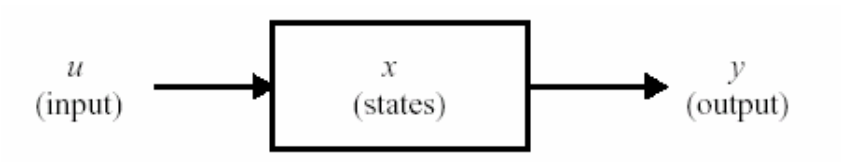

The mathematical relationship between them can be expressed as:

$$
\begin{aligned}
y &= f_0(t, x, u) && \text{(output)} \\
x_c &= f_d(t, x, u) && \text{(derivative)} \\
x_{d_{k+1}} &= f_u(t, x, u) && \text{(update)} \\
&where \quad x = x_c + x_d
\end{aligned}
$$

1, S-Function

As other Simulink blocks, the s-function block proceeds in stages. It initializes before

entering the simulation loop, where each pass through the loop is referred to as a simulation step (time step in our case). During each simulation step, the function would compute the states, derivatives, and outputs for the current sample time. So on and so forth, until the simulation is complete.

2, Simin

Simin is another main Simulink block employed in the model. This block, when connected with the s-function block, can import the data in workspace, making data serve as input to the block.

In this model, the ambient temperature, process air inlet temperature and the exhaust gas inlet temperature that were acquired from the experiment serve as inputs to the model so that the system's response to real-time changes can be observed better. The experimental data, as stated before, were acquired on a minute-by-minute basis, and were interpolated in a way that a reasonable value can be obtained at any time when being imported into the model.

Results and Discussions

Below is a set of simulation results obtained, some of them were compared with the experimental data.

The experimental data used here comes from a typical summer day's experiment; they are being collected by the HP VEE system introduced previously, on a minute-by-minute basis. They are not exactly the same as the simulation results since the exact manufacturer's parameters that have been assumed in the program were not available to us, and the cooling water fan's effects, which cause these fluctuations of the chilled water temperature as shown in the plots, have not been taken into account in this simulation either. So, the main purpose of the comparison here is to validate the transient trend, and that matches well between the experimental data and simulation results. In all the figures where there is comparison between experimental data and simulation results, the experimental data are all plotted in dots, while the simulation results are plotted in lines.

It can be observed that the chiller reaches its full capacity after about 100 minutes as shown in Figure 48. The return temperature and supply temperature of the chilled water start at the same point when the machine starts. In the first 18 minutes or so, when the chiller has not yet started to provide cooling, due to heat loss during the circulation, the supply water's temperature became a little bit higher than the return water's. Then they reverse and behave as expected. The other item that is noticed are the fluctuations on the experimental data plots, these result from the cooling tower fan cycling. In real operations, cooling fan for the cooling tower is controlled in a way that when the cooling water return temperature exceeds a certain set point, the cooling fan turns on to lower it. By doing so, the cooling water's temperature is

controlled and the effect of it is refelcted in the fluctuations. However, the cooling fan effect is omitted in our simulation.

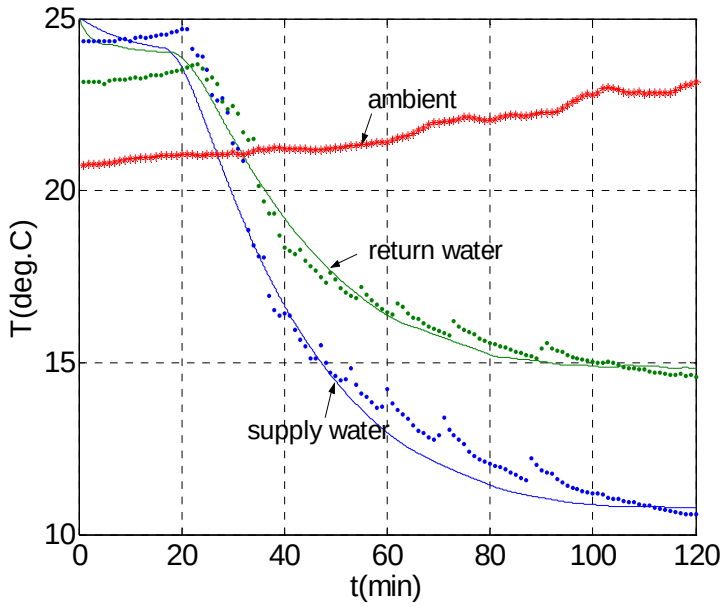

Figure 48 Chilled Water Temperature Profile

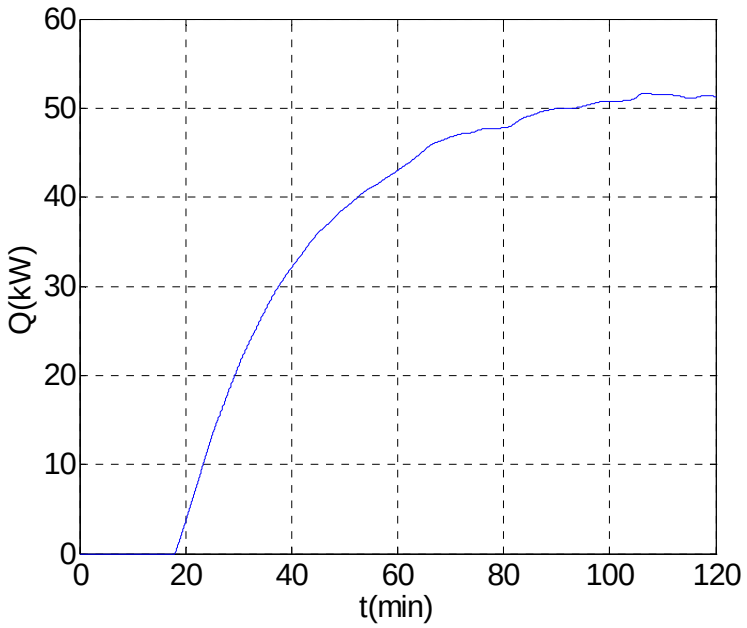

Figure 49 Cooling Capacity Profile

Corresponding to the water temperatures above, the plot of the cooling capacity's change with time is shown above. It starts with providing no cooling capacity for the initial 18 minutes or so and increases with time, until it reaches its full capacity.

The reason of this delay can be explained with Figure 50, in which the solution temperatures at different points of the chiller, as well as the temperature of the components are shown.

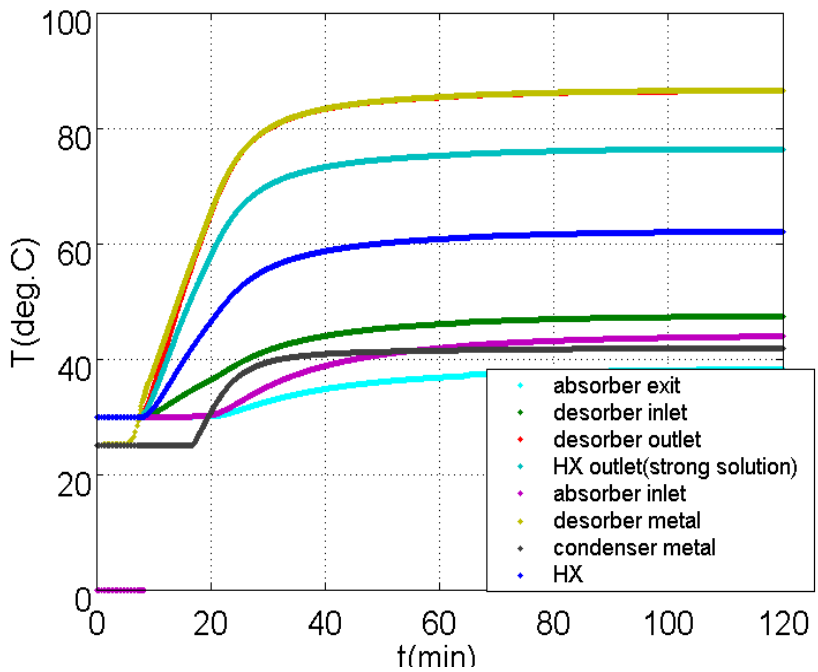

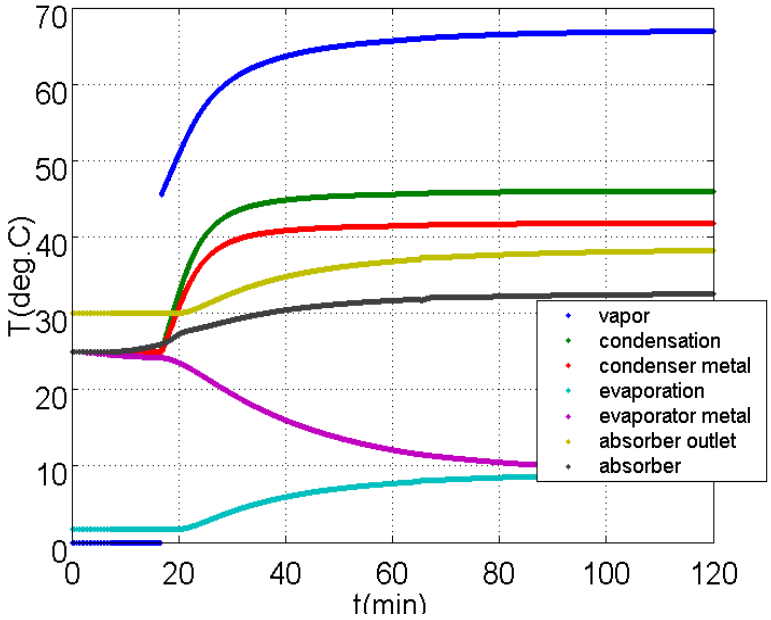

Figure 50 Chiller Temperature Profiles

As shown above, the solution temperatures all kept constant for about 10 minutes and rose up gradually after that, while the temperature of the evaporator metal goes down after 18 minutes, due to the cooling provided by the vapor.

In the first 18 minutes, energy are being stored into the desorber metal, as well as the solution in the desorber, yet it is not enough to raise the solubility of LiBr to beyond the saturation concentration under the high pressure, so that no vapor is generated then, and so no cooling could be provided. After this period, both the desorber metal and solution stored in the desorber are hot enough that vapor starts to be generated and cooling is provided, that's when the chilled water supply temperature starts to go

down.

Figure 51 shows the high stage and low stage pressures. High stage pressure keeps constant for the first 18 minutes, during which no vapor is generated; and then increases as the strong solution's temperature and vapor temperature rise. Also, the low stage pressure also increases about 50% of the initial value due to energy storage in the weak solution.

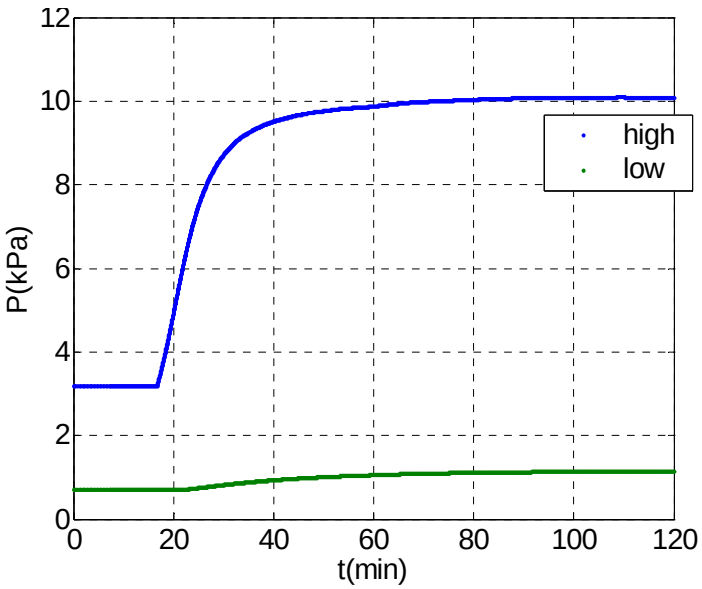

Figure 51 Chiller Pressure Profile

The concentration of the strong solution is as shown in the following graph. It is constant when no vapor is generated, and goes up as the amount of vapor generated becomes bigger.

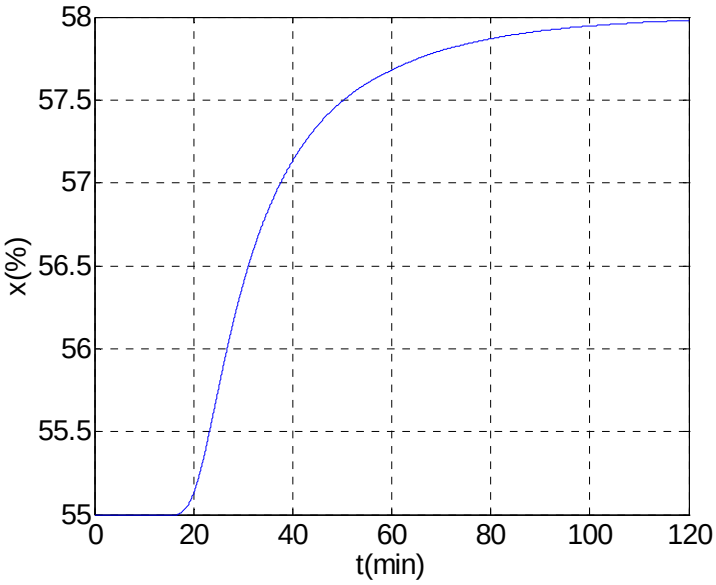

Figure 52 Concentration of Strong Solution

The outlet temperature of the exhaust gas has also been simulated in the program, and it shows good accordance with the experimental data as well. The exhaust outlet temperature goes up really fast during the first 20 minutes or so, during this process, the temperature of the desorber and its solution go up really fast as well, so that the temperature difference between the exhaust and the desorber becomes smaller that the heat that can be transferred into the desorber becomes less, and the exhaust outlet temperature rises. It stabilizes after about 100 minutes.

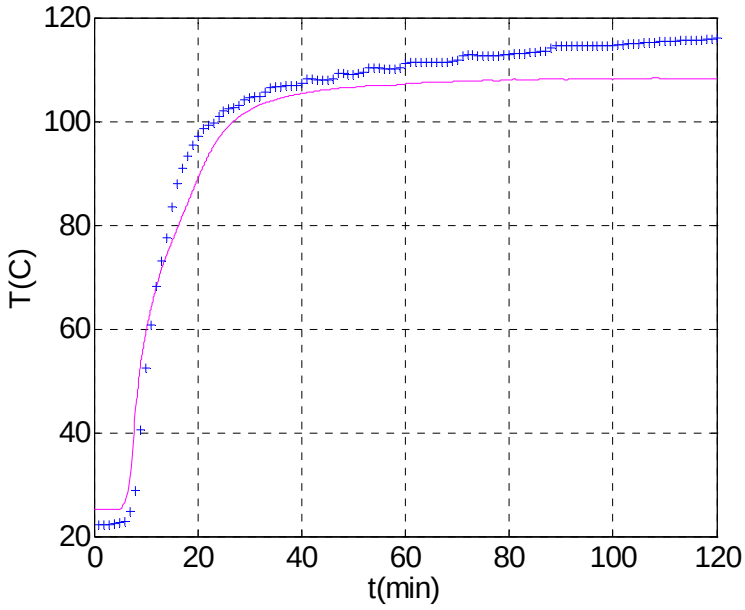

Figure 53 Exhaust Gas Outlet Temperature

6 Conclusions

Two main investigations on CHP equipment performance have been done in this study: CHP system fuel flexibility analysis and transient process simulation.

MT Fuel Flexibility

From the results obtained in field tests, the performance of the 60 kW MT on both natural gas and propane has been summarized. The results and analysis are listed as below:

1. Both fuels provided steady and reliable operation of the microturbine
2. The power output from both fuels can reach the full capacity of 60kW, and decreases as the ambient temperature/compressor inlet temperature increases, resulting from the limit of the engine speed
3. Running on propane caused more parasitic power consumption by the compressor due to the larger than expected flow rate of propane, and possibly to the design of the compressor.
4. The performance efficiency when running on propane is lower than that on natural gas. This comes from the pre-set program of the fuel control device, which was designed for another type of microturbine that has different gas intake pressures. This control program resulted in more fuel consumption than actually needed, thus lowering the efficiency.

The efficiency reduction can be corrected with a new control program.

5. Although having a lower efficiency, the microturbine produced more exhaust heat when running on propane. From this observation, a suggestion of a power generation device that can adjust its exhaust heat output by controlling fuel consumption to meet variable heating/cooling loads of the building while maintaining a constant power output has been made.

Absorption Chiller Transient Simulation

A transient model of a LiBr-Water absorption cooling cycle has been developed.

By using MATLAB Simulink®, a variable time step is adopted, which ensures the accuracy of the simulation, while saving computation time.

The ambient air temperature, exhaust gas inlet temperature and the return air temperature that served as the inputs of the above model are a set of minute-by-minute data acquired from the experiment on a typical summer day.

By using the above model, reasonable transient trends of the start-up process of an absorption chiller in a CHP system have been achieved.

7 References

1. Jalalzadeh-Azar, A., A parametric analysis of a grid-independent BCHP system – focusing on impact of technological advancements, ASHRAE Transaction 2003

2. Shibata, S., Inoue, U., Abe, H., Tanaka, T., 2001: Development and Operation of Microturbine – Combined Package of Steam Generator with Supplemental Firing. Japan Tappi Journal, v55, n5, May 2001, 2001, p 30-33

3. Khan, K.H., Rasul, M.G., Khan, M.M.K., Energy conservation in buildings: cogeneration and cogeneration coupled with thermal-energy storage. Applied Energy 77(2004) 15-34

4. Kaarsberg, T., Roop, J., Combined Heat and Power: How Much Carbon and Energy Can It Save for Manufacturers? IECEC-98-I209 33rd, Intersociety Engineering Conference on Energy Conversion, Colorado Springs, CO, 1998

5. Gomes, E.E.B., et al, Case studies of distributed generation projects with microturbines in Brazil, International Joint Power Generation Conference, summer 2003

6. Cowie, M., Liao, X., Second generation integrated microturbine, absorption chiller and solid desiccant system, International Congress of Refrigeration, 2003

7. Strachan, N. Farrell, A., Emissions from distributed vs. centralized generation: The importance of system performance, Energy Policy, 2005-7-8

8. Mone, C.D., Chau, D.S., Phelan, P.E., Economic feasibility of combined heat and

power and absorption refrigeration with commercially available gas turbines, Energy Conversion and Management 42 (2001) 1559-1573

9. Smith, M.A., et al, Technical and operational performance of a small-scale, combined heat-and-power (CHP) plant, Energy, Vol. 20, No.12, pp 1205-1214, 1995

10. Liao, X., Ph.D. Dissertation: The development of an air-cooled absorption chiller concept and its integration in CHP systems, University of Maryland, 2004

11. Cowie, M, Liao, X., Applying CHP to the ventilation air of the buildings, Proceeding of IMECE'03, ASME International Mechanical Engineering Congress & Exposition, 2003

12. Cowie, M., Master Thesis: Characterizing combined heating, cooling and power systems for buildings through theory and testing, University of Maryland, 2002

13. Alefeld, G., Radermacher, R., Heat conversion systems, CRC Press, Boca Raton, Florida, 1993.

14. Herold, K., Radermacher, R., and Klein S., Absorption chillers and heat pumps, CRC Press, Boca Raton, FL, 1996

15. Rizy, D. T., Zaltash, A., et la, CHP integration (or IES): Maximizing the efficiency of distributed generation with waste heat recovery, Proceedings of the Power Systems 2003 Conference, Clemson, SC, March, 2003

16. Rizy, D. T., et al, DER performance testing of a microturbine-based combined cooling, heating, and power (CHP) system, Proceedings of Power System 2002

conference, Clemson, SC March 2002

17. Marantan, A., Ph.D. Dissertation: Optimization of integrated microturbine and absorption chiller systems in CHP for buildings applications, University of Maryland, 2002

18. Sanders R., What Is So Attractive about Microturbines? Powerline Magazine, November/December, 1998

19. Capstone C60 Product Sheet http://www.capstoneturbine.com

20. Natural Gas Characteristics http://www.unctad.org

21. Department of Energy http://www.eere.energy.gov/de/thermally_activated/tech_basics.html

22. Florides, G.A., Kalogirou, S.A., Tassou, S.A. and Wrobel, L.C. Design and construction of a LiBr-water absorption machine. Energy Conversion and Management 44. 2003

23. Jeong, S., Kang, B. H. and Karng, S. W. Dynamic simulation of an absorption heat pump for recovering low grade waste heat. Applied thermal engineering, vol.18, 1998

24. Bian, J., Radermacher, R., and Moran, D., Transient simulation of an absorption chiller in a CHP system, International Sorption Heat Pump Conference, Summer 2005

25. Jeong, S., Kang, B. H. and Karng, S. W. , Computer simulation on dynamic behavior of a hot water driven absorption chiller, International Absorption Heat Pump Conferece, ASME 1993, AES-Vol. 31

26. Kim, Minsung, Kim, Min Soo, Chuang, Jae Dong. Transient thermal behavior of a water heater system driven by a heat pump. International Journal of Refrigeration 27, 2004.

27. Chua, H.T., Toh, H.K., Ng, K.C., Thermodynamic modeling of an ammonia-water absorption chiller, International Journal of Refrigeration 25, 2002.

28. Dence, A.E., Nowak, C.C., Perez-Blanco, H., A transient computer simulation of an ammonia-water heat pump in cooling mode, IEEE 1996.

29. Broad Absorption Chiller Product Sheet